University of Groningen

Tomographic intensity mapping versus galaxy surveys

Silva, Marta B.; Zaroubi, Saleem; Kooistra, Robin; Cooray, Asantha

Published in:
Monthly Notices of the Royal Astronomical Society

DOI:
10.1093/mnras/stx3265

IMPORTANT NOTE: You are advised to consult the publisher's version (publisher's PDF) if you wish to cite from it. Please check the document version below.

Document Version
Publisher's PDF, also known as Version of record

Publication date:
2018

Link to publication in University of Groningen/UMCG research database

Citation for published version (APA):
Silva, M. B., Zaroubi, S., Kooistra, R., & Cooray, A. (2018). Tomographic intensity mapping versus galaxy surveys: observing the Universe in H alpha emission with new generation instruments. Monthly Notices of the Royal Astronomical Society, 475(2), 1587-1608. https://doi.org/10.1093/mnras/stx3265

Copyright
Other than for strictly personal use, it is not permitted to download or to forward/distribute the text or part of it without the consent of the author(s) and/or copyright holder(s), unless the work is under an open content license (like Creative Commons).

Take-down policy
If you believe that this document breaches copyright please contact us providing details, and we will remove access to the work immediately and investigate your claim.

Downloaded from the University of Groningen/UMCG research database (Pure): http://www.rug.nl/research/portal. For technical reasons the number of authors shown on this cover page is limited to 10 maximum.

Download date: 29-04-2019

Monthly Notices of the ROYAL ASTRONOMICAL SOCIETY

MNRAS **475,** 1587–1608 (2018)
Advance Access publication 2017 December 20

doi:10.1093/mnras/stx3265

Tomographic intensity mapping versus galaxy surveys: observing the Universe in H α emission with new generation instruments

Marta B. Silva,[1★] Saleem Zaroubi,[1,2,3] Robin Kooistra[1] and Asantha Cooray[4]

[1] *Kapteyn Astronomical Institute, University of Groningen, Landleven 12, NL-9747AD Groningen, the Netherlands*
[2] *Department of Natural Sciences, The Open University of Israel, 1 University Road, PO Box 808, Ra'anana 4353701, Israel*
[3] *Department of Physics, The Technion, Haifa 32000, Israel*
[4] *Department of Physics & Astronomy, University of California, Irvine, CA 92697, USA*

Accepted 2017 December 14. Received 2017 December 14; in original form 2017 July 5

ABSTRACT

The H α line emission is an important probe for a number of fundamental quantities in galaxies, including their number density, star formation rate (SFR), and overall gas content. A new generation of low-resolution intensity mapping (IM) probes, e.g. SPHEREx and CDIM, will observe galaxies in H α emission over a large fraction of the sky from the local Universe till a redshift of $z \sim 6 - 10$, respectively. This will also be the target line for observations by the high-resolution *Euclid* and *WFIRST* instruments in the $z \sim 0.7$–2 redshift range. In this paper, we estimate the intensity and power spectra of the H α line in the $z \sim 0$–5 redshift range using observed line luminosity functions (LFs), when possible, and simulations, otherwise. We estimate the significance of our predictions by accounting for the modelling uncertainties (e.g. SFR, extinction, etc.) and observational contamination. We find that IM surveys can make a statistical detection of the full H α emission between $z \sim 0.8$ and 5. Moreover, we find that the high-frequency resolution and the sensitivity of the planned CDIM surveys allow for the separation of H α emission from several interloping lines. We explore ways to use the combination of these line intensities to probe galaxy properties. As expected, our study indicates that galaxy surveys will only detect bright galaxies that contribute up to a few per cent of the overall H α intensity. However, these surveys will provide important constraints on the high end of the H α LF and put strong constraints on the active galactic nucleus LF.

Key words: dust, extinction – galaxies: high-redshift – galaxies: ISM – galaxies: star formation – submillimetre: galaxies.

1 INTRODUCTION

The H α line is frequently used to detect star-forming galaxies and quasars at low to medium redshifts ($z \lesssim 2.3$). Thanks to its weak metallicity dependence, its relatively high luminosity and favorable observing frequency (relative to the Ly α line), H α is the main target line of several new space instruments. Due to their very large survey volumes, this new generation of instruments will revolutionize the study of the global properties of galaxy formation and evolution and put very stringent constraints on dark energy models (Gehrels et al. 2015; Amendola et al. 2013).

Being a hydrogen recombination line, H α emission is dominated by massive, short-lived stars, such as type O stars and early-type B stars, characterized by time-scales <10–20 Myr. Hence, it is a good tracer of the instantaneous SFR (Lee et al. 2009; McQuinn et al. 2015). To constrain the H α intensity, a proper sampling of the high-mass end of the initial mass function is required to overcome cosmic variance. In addition, accounting for medium luminosity systems, which also contribute significantly to the overall line intensity requires both large volumes and relatively high sensitivities (Sobral et al. 2015; Pozzetti et al. 2016).

At low redshift, $z \lesssim 2.3$, the dust attenuation of H α flux is of the order of 1 mag (Sobral et al. 2013, 2016b). However, it is expected to decline at higher redshifts, given the lower dust content of the interstellar medium (ISM). Furthermore, both the observed and intrinsic H α line emissions correlate well with the overall galaxy luminosity. In contrast, other metal UV lines, such as [O III]500.7 nm or [O II]372.7 nm, depend strongly on the metallicity and dust content of the galaxy (Khostovan et al. 2015).

In recent years, a method for probing gas in the Universe, called Intensity Mapping, has been proposed (Madau, Meiksin & Rees 1997). The basic idea is to observe the intensity of a specific line emission, e.g. H I 21 cm radiation (Madau et al. 1997; Chang et al. 2010; Masui et al. 2013), and map it at every point in space and

★ E-mail: silva@astro.rug.nl

© 2017 The Author(s)
Published by Oxford University Press on behalf of the Royal Astronomical Society

Downloaded from https://academic.oup.com/mnras/article-abstract/475/2/1587/4768282 by University of Groningen user on 20 March 2019

redshift, down to the resolution and sensitivity of the telescope. Since this method probes a certain spectral line, the redshift of the observed gas parcel comes for free. Therefore, the 3D mapping made available by this method contains an enormous amount of information about the integrated galaxy and IGM emission from each voxel. This new technique is expected to provide a wealth of information that is not yet available to current probes. For example, using intensity mapping (IM) surveys in combination with galaxy surveys will link the distribution of galaxies with IGM overdensities. Given its simplicity and many advantages, IM has been extended to several other atomic and molecular emission lines, such as CO, C II, and Ly α, used to probe the Epoch of Reionization (Visbal & Loeb 2010; Lidz et al. 2011; Gong et al. 2012; Silva et al. 2013, 2015). Moreover, IM has also been proposed as a probe of the medium to low redshift Universe in several lines (Pullen, Doré & Bock 2014; Uzgil et al. 2014; Silva, Kooistra & Zaroubi 2016; Fonseca et al. 2017).

Recently, two H α IM instruments have been proposed. The first is SPHEREx (the Spectrophotometer for the History of the Universe, Epoch of Reionization, and Ice Explorer), which is a NASA Medium-Class Explorer mission selected for phase A study in 2017 (Doré et al. 2014, 2016). The second instrument is CDIM (the Cosmic Dawn Intensity Mapper; Cooray et al. 2016) space telescope. Fonseca et al. (2017) have explored the use of the surveys of these two instruments to constrain cosmological models. They found that these missions are able to constrain the H α power spectrum at $k > 0.02\,h\,\mathrm{Mpc}^{-1}$ down to the few per cent accuracy. This makes them useful for probing the baryonic acoustic oscillations (BAO) scale. Furthermore, Gong et al. (2017) have demonstrated the potential of SPHEREx to put strong constraints on the star formation rate density (SFRD) for $z \lesssim 5$, assuming that it scales linearly with the observed H α intensity and overlooking the contamination by background lines in the H α intensity maps.

Two other interesting instruments for H α studies are the *Euclid* (Laureijs et al. 2011) and *WFIRST* (*Wide − FieldInfraredSurveyTelescope*; Green et al. 2012; Spergel et al. 2015) space telescopes. This new generation of instruments will carry out galaxy surveys in a very wide area, particularly compared to ground-based instruments. Their spectroscopic capabilities will provide data with high-frequency resolution to allow the distinction between two lines with small frequency separation, hence significantly reducing line contamination (Pozzetti et al. 2016). Although their spectroscopic sensitivity is low, these telescopes will have high photometric sensitivity that will allow them to probe down to faint sources – fainter than the best available ground-based instruments.

We note here that these two instruments will not carry out IM surveys. Furthermore, the wide-band filters used by *Euclid* and *WFIRST* will result in a poor determination of the emitted line and thus of the galaxy redshift. Spectroscopic follow-up of the photometric sources will only be possible for a few cases and usually for relatively bright galaxies. Another option would be to use IM surveys, covering the same area of the sky, to provide better redshift estimates for these galaxies.

In this paper, we study the H α emission at $z \lesssim 5$ expected to be observed by these four instruments. We improve upon previous predictions by estimating the uncertainty in the intensity of the intrinsic H α signal and of the dust extinction suffered by H α photons. We also account for the contribution of quasars to the overall H α luminosity density. Moreover, we explore several possible constraints on astrophysical quantities obtained from the surveys targeting H α emission.

We investigate the contamination of the relevant background/foreground lines in H α intensity maps at each redshift. These interloping lines include the hydrogen H β (486.1 nm) and Ly α (121.6 nm) lines, the [S II] (671.7 nm)(673.1 nm) doublet, the [N II] (658.3 nm)(654.8 nm) doublet and the ionized oxygen [O II] (372.7 nm) and [O III] (500.7 nm) lines. By doing this study using simulations, we are able to self-consistently explore the foreground removal technique needed to recover the H α signal from observational intensity maps.

The paper is organized as follows. In Section 2, we present the physical processes that give rise to the observed H α line luminosity in galaxies. In Section 3 we present and discuss current constraints on the galaxy H α LF, and on the SFR-halo mass relation. The simulation code we run in order to predict the intensity and spatial fluctuations of H α emission from both galaxies and the IGM is presented in Section 4. We follow by describing the four instruments and their planned H α survey characteristics in Section 5. In Sections 6 and 7, we discuss foreground removal strategies in H α intensity maps in the context of these instruments. A comparison between constraints from galaxy and IM surveys is made in Section 8. The final conclusions are presented in Section 9.

Throughout this paper we assume the best-fitting cosmological parameters from *Planck* + WMAP (Planck Collaboration XVI 2014) ($\Omega_b h^2 = 0.022032$, $\Omega_m = 0.3089$, $h = 0.6704$, $Y_P = 0.2477$, $n_s = 0.9619$, and $\sigma_8 = 0.8347$).

2 H α PHYSICS: FROM SFR TO LINE LUMINOSITY

The H α line is a Balmer line that corresponds to a transition between energy levels $n = 3$ to $n = 2$ of neutral hydrogen. It is predominantly emitted during hydrogen recombinations, but can also arise due to collisional excitation of this transition. The latter process is mainly relevant for warm and neutral gas, such as the boundary region between ionized and neutral gas. Therefore, recombination emission usually dominates the overall H α emission in galaxies (Cantalupo, Porciani & Lilly 2008).

It is commonly assumed that the volume average escape fraction of ionizing photons, from galaxies, is very small. This quantity is poorly constrained from observations. However, in the few cases where it has been measured (along a few lines of sight), it is found to be below the 10 per cent level (Vasei et al. 2016). The escape fraction of ionizing photons is highly dependent on the gas conditions in the ISM. It can thus range from almost zero up to a few tens of percents. High values of escape fraction are a signal that the ISM contains low-column density channels along which ionizing photons can easily escape. Given the current results from simulations and observations, in the relevant redshift range, escape fractions above 10–20 per cent are unlikely (Boutsia et al. 2011; Yajima et al. 2014). As a first approximation, and given that this parameter is degenerate with the galaxy SFR, we will assume that it is zero. The number of hydrogen atom ionizations can then be inferred from the stellar emission spectrum of the galaxy. It should be noted that a zero escape fraction is the common assumption in the estimation of the SFRD from observations of nebular emission lines (Geach et al. 2008; Suzuki et al. 2016).

Following Kennicutt (1998b), we connect the SFR to the galaxy luminosity (L_ν) in the 1500–2800 Å wavelength range by averaging over a Salpeter (1955) initial mass function (IMF) with solar metallicity and with mass limits 0.1–100 $\mathrm{M}_\odot$. This gives

$$\mathrm{SFR}(\mathrm{M}_\odot\,\mathrm{yr}^{-1}) = 1.4 \times 10^{-28}\, L_\nu\,(\mathrm{ergs\,s^{-1}\,Hz^{-1}}). \quad (1)$$

Downloaded from https://academic.oup.com/mnras/article-abstract/475/2/1587/4768282 by University of Groningen user on 20 March 2019

Taking the population synthesis galaxy spectra from Bruzual & Charlot (1993), we relate the luminosity density at 1500 Å to the rate of hydrogen ionizing photon emission ($Q_{\rm H}$). This yields the following relation:

$$\mathrm{SFR}(\mathrm{M}_\odot\,\mathrm{yr}^{-1}) = 1.08 \times 10^{-53}\, Q_{\rm H}\,(\mathrm{s}^{-1}), \tag{2}$$

which is valid for star formation in the age interval 0.1–1 Gyr, dictated by the assumed IMF.

The time-scale for hydrogen ionization is of the order of a few years and the time-scale for recombination in the dense ($n \sim 10^2$–$10^4\,\mathrm{cm}^{-3}$) and ionized ISM is of the order of few hundred years. From a cosmological point of view, these are instantaneous processes. Hence, one can safely assume ionization-recombination equilibrium.

For a case B recombination coefficient (the choice of recombination coefficient has little impact on this result), an average gas temperature of 10^4 K will result in the emission of ∼0.45 H α photons per hydrogen recombination (Osterbrock 1989; Madau et al. 1996). This results in the commonly used relation between SFR and the intrinsic H α luminosity (Kennicutt 1998a):

$$L_{\rm H\alpha}^{\rm int}\,(\mathrm{erg\,s}^{-1}) = 1.26 \times 10^{41}\, SFR\,(\mathrm{M}_\odot\,\mathrm{yr}^{-1}). \tag{3}$$

Ideally, one should choose the IMF according to the target population. However, this information is usually not available, which introduces IMF-related uncertainty into our calculations. For example, using a Kroupa IMF (Kroupa & Weidner 2003) or a Chabrier IMF (Chabrier 2003) would result in an increase of ∼1.54–1.64 in the $L_{\rm H\alpha}^{\rm int}/SFR$ ratio compared to the Salpeter IMF. Additional uncertainty in this relation arises from the choice of population synthesis galaxy spectra (Lee et al. 2009).

The observed H α luminosity is obtained by correcting the intrinsic luminosity for dust extinction. This extinction is usually taken to be of the order of $A_{\rm H\alpha} = 1$ mag, defined as:

$$L_{\rm H\alpha}^{\rm obs} = L_{\rm H\alpha}^{\rm int} \times 10^{-A_{\rm H\alpha}/2.5}. \tag{4}$$

Dust extinction increases with stellar mass and environment density (Sobral et al. 2016b). The amount of dust, and therefore its line extinction power, correlates with metallicity and is expected to decrease with increasing redshift.

The steep increase of the extinction with stellar mass has a strong impact on the overall extinction, affecting surveys with different flux sensitivity. The commonly used extinction value, $A_{\rm H\alpha} = 1$ mag, corresponds to galaxies with stellar masses of a few times $10^{10}\,\mathrm{M}_\odot$ (Sobral et al. 2016b). From semi-analytical studies (Mitchell et al. 2016), the dark matter halo masses corresponding to these stellar masses straddle two orders of magnitude, centred at $M_{\rm halo} \sim 10^{12}\,\mathrm{M}_\odot$. Due to their sensitivity limits, *Euclid* and *WFIRST* spectroscopic surveys will only be able to observe these luminous and massive galaxies. Therefore, for these surveys the extinction value of $A_{\rm H\alpha} = 1$ mag is appropriate. However, for surveys capable of probing low-luminosity galaxies, the overall extinction might be smaller.

Note that H α emission will also suffer extinction due to the dust in the Milky Way. This decrement in the H α flux can be estimated with dust maps of the Milky Way. As a reference, corrections due to interstellar extinction in the COSMOS field, in the relevant frequency bands for this study, are of the order of $\lesssim$0.05 mag (Capak et al. 2007). Moreover, intensity maps will need to be corrected for continuum galactic dust emission and zodiacal light (Schlegel, Finkbeiner & Davis 1998).

Unlike Ly α, H α photons are not efficiently absorbed by neutral hydrogen. Therefore, their flux is expected to suffer little to no attenuation due to scattering or dust extinction along their path through to the IGM.

3 MODELLING H α EMISSION

3.1 H α constraints from observational LFs

We make use of the H α LFs compiled by Pozzetti et al. (2016). These include data from the ground-based imaging Hi-Z Emission Line Survey (HiZELS) with UKIRT, Subaru and VLT (Sobral et al. 2013), the WISP slitless space-based spectroscopic survey (Colbert et al. 2013) with the Wide Field Camera 3 on HST (HST+WFC3) and from the HST Near Infrared Camera and Multi-Object Spectrograph (HST-NICMOS) (Shim et al. 2009; Hopkins, Connolly & Szalay 2000; Yan et al. 1999).

For simplicity, we fit the H α LF using a Schechter fitting function (Schechter 1976):

$$\Phi(L)\mathrm{d}L = \phi_* \left(\frac{L}{L_*}\right)^{\alpha} \exp\left(-\frac{L}{L_*}\right)\frac{\mathrm{d}L}{L_*}, \tag{5}$$

where ϕ_* is a normalization factor with units of inverse volume, L_* is the characteristic luminosity at which there is a break in the luminosity function, and α is the faint-end slope. This formula usually applies to the intrinsic continuum luminosity of galaxies. However, it has also been shown to be a good fit to galaxy line luminosities. In the case of the H α line LF, it reproduces the emission from star-forming galaxies well, but not the additional contribution from active galactic nucleus (AGN). The observed line luminosity function is then better described by a Schechter fitting function plus a power law (Matthee et al. 2017).

Alternatively, these observations can be fitted to other functions, such as the Saunders et al. (1990) fitting function. Therefore, one should bear in mind that the choice of using Schechter fitting function can introduce certain biases to our estimates.

We evolve the H α LF in the redshift range $0 < z < 2.3$ following the observed LFs mentioned above. Given the small number of H α flux observations at higher z, we infer the H α luminosity from observed UV fluxes following the method described in Smit et al. (2016). Basically, this method consists of converting the LFs at 1600 Å into SFRs and then to H α luminosities using equations (1) and (3), respectively.

We consider two prescriptions for the H α dust extinction. In the first case, we assume an H α dust extinction of $A_{\rm H\alpha} = 1$ mag for the entire redshift range. While in the second case we assume an H α dust extinction of $A_{\rm H\alpha} = 1$ mag for the low z ($z \lesssim 2.3$) sample and a decreasing extinction towards high z, reaching $A_{\rm H\alpha} = 0.475$ mag at $z \sim 5$. The latter extinction value is obtained by requiring the UV data to fit the H α LFs. The high z constraints on the H α LF are based on the offset between 3.6 μm fluxes from *Spitzer*/IRAC and the best spectral energy distribution (SED) fits from the HST upper limits and the *Spitzer*/IRAC photometry (Smit et al. 2016).

The observed low-z H α LFs include emission from both star-forming galaxies and AGNs. The percentage of H α emitters powered by AGN activity depends on the luminosity limits. It can range from a few tens of percent in luminous galaxies to practically zero for faint galaxies. For example, Sobral et al. (2016a) have measured an AGN contribution of 30 ± 8 per cent in the redshift range $z \sim 0.8$–2.23 for bright galaxies ($L_{\rm H\alpha} > L_*$).

The mean intensity of H α emission is

$$\bar{I}_{\rm H\alpha}(z) = \int_{L_{\rm min}}^{L_{\rm max}} \mathrm{d}L \frac{\mathrm{d}n}{\mathrm{d}L} \frac{L_{\rm H\alpha}}{4\pi D_{\rm L}^2}\, y(z) D_{\rm A}^2, \tag{6}$$

Downloaded from https://academic.oup.com/mnras/article-abstract/475/2/1587/4768282 by University of Groningen user on 20 March 2019

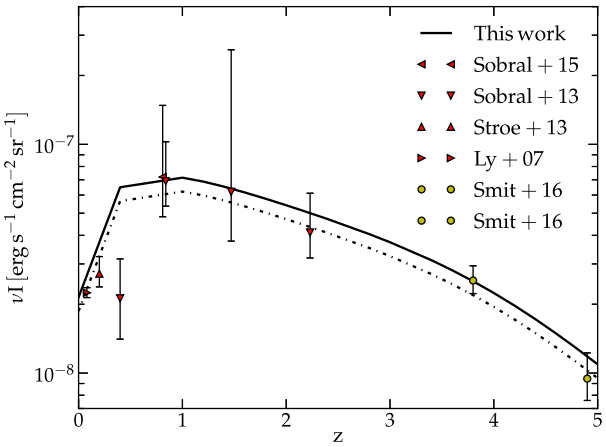

Figure 1. Intensity of observed Hα emission from galaxies. The red triangles correspond to observed Hα fluxes at $z \lesssim 2.3$ (Gallego et al. 1995; Sobral et al. 2013, 2015; Stroe & Sobral 2015). At higher z, yellow symbols correspond to Hα intensities obtained from the offset between 3.6 μm fluxes from *Spitzer*/IRAC and best SED fits from HST upper limits and *Spitzer*/IRAC photometry, following Smit et al. (2016). The latter correspond to star-forming Hα emitters only. Also shown is the fit to the observational points based on the Cole et al. (2001) SFRD fitting formula, with (solid line) and without (dotted line) assuming an intensity boost of 15 per cent due to AGN-powered Hα emission. Error bars corresponding to the one-sigma uncertainty on the low-luminosity end slope of the observational LFs.

where $D_{\rm L}$ is the proper luminosity distance, $D_{\rm A}$ the comoving angular diameter distance, and $y(z)[{\rm Mpc}\,h^{-1}\,{\rm Hz}^{-1}] = {\rm d}\chi/{\rm d}\nu$, where χ is the comoving distance. In galaxy surveys, the lower luminosity limit, $L_{\rm min}$, is set by the sensitivity of the instrument. However, the mean intensity due to the whole Hα population would require $L_{\rm min} = 0$. The contribution of very faint galaxies, i.e. more than two or three orders of magnitude below L_*, to the total line intensity is quite small for all possible LF shapes. The choice of the upper limit in luminosity for the integration, $L_{\rm max}$, should be the same for any survey. It is usually taken as the maximum observed luminosity, which is a few orders of magnitude above L_* (Pozzetti et al. 2016).

The constraints on the mean intensity of Hα emission from observational LFs are shown as symbols in Fig. 1. Also shown is the best fit to the observational data derived from the Cole et al. (2001) SFRD fitting function (black lines). The solid and dashed-dotted lines denote the Hα intensity with and without a 15 per cent boost due to the presence of AGN, respectively (Garn & Best 2010; Sobral et al. 2013). The intensity points were derived by integrating the observed luminosity functions down to Hα fluxes of 10^{30} erg s^{-1}, which is well below the observed flux limit. We fixed this lower flux limit and determined the one-sigma error bars from the one-sigma uncertainty in the low-luminosity end slope. Given that this model fits the observational constraints well, it will be our base model. The total Hα intensity (including the AGN contribution) corresponding to this fit is

$$\bar{I}_{\rm H\alpha}(z) = 2.892 \times 10^{-9} \frac{0.027 + 0.28z}{1 + (z/4.8)^{5.3}} \frac{(1+0.15)}{(1+z)^2} \times \frac{y(z)}{[{\rm Mpc}}\, h^{-1}\,{\rm Hz}^{-1}]\,{\rm erg\,s^{-1}\,cm^{-2}\,sr^{-1}\,Hz^{-1}}. \quad (7)$$

We will further discuss this model in Section 3.2. The uncertainties in the model will be discussed in Section 8.

Table 1. Fitting parameters for the SFR–halo mass relation.

	$z = 0$	$z = 0.8$	$z = 1$	$z = 2.2$	$z = 4.8$
a	−9.3	−8.75	−8.75	−8.2	−6.7
b	2.6	2.7	2.7	2.7	2.5
c	−2.9	−3.0	−3.0	−2.95	−2.6
$\log_{10} M_2$	11.9	11.7	11.7	11.6	11.3

3.2 Hα bias constraints from simulations

We make use of an SFR model based on simulations, in order to predict Hα line luminosities where they are not observationally available. This is usually the case at higher redshifts and/or at low line luminosities. The use of simulations, which provide a relation between SFR and halo mass, will also allow us to estimate the Hα bias needed to compute the line power spectra. In this section, we compare how well different analytical functions are able to reproduce our simulated and observational constraints. We choose the best of these fits as our base SFR/SFRD model.

3.2.1 SFR

We adopt the catalogue of Guo et al. (2013) (hereafter, Guo2013), who used a semi-analytic prescription that incorporates astrophysical properties of the Sloan Digital Sky Survey (SDSS) to the dark matter haloes in the Millennium and Millennium II cosmological simulations (Springel et al. 2005; Boylan-Kolchin et al. 2009). This catalogue includes an estimate of the galaxy SFR based on its cold gas mass, the fuel for star formation. It is assumed that during a single orbital period, 20 per cent of the cold gas in the galaxy is converted into stars. This is usually presented as the galaxy having an $\epsilon = 0.2$ efficiency per dynamical cycle of converting cold gas into stars. The average of the star formation in these galaxies as a function of halo mass can be parametrized with the function

$$\mathrm{SFR}(M) = 10^a \left(\frac{M}{M_1}\right)^b \left(1 + \frac{M}{M_2}\right)^c \ [\mathrm{M_\odot\,yr^{-1}}], \quad (8)$$

where $M_1 = 10^8\,\mathrm{M_\odot}$. The remaining fitting parameters for redshifts ranging from $z \sim 0$ to 4.8 can be found in Table 1. This fit is valid in the $M \sim (10^8\text{–}10^{13})\,\mathrm{M_\odot}$ mass range for $z < 4$ and in the $M \sim (10^8\text{–}10^{12})\,\mathrm{M_\odot}$ mass range for $z \gtrsim 4$. At higher halo masses, the SFR is assumed to be constant. As an example, Fig. 2 shows this relation at $z = 2.2$. In Section 3.2.2 we discuss a normalization to this relationship that we applied in order to better fit current observational constraints.

3.2.2 SFRD

It is worth pointing out the large uncertainties in the evolution of the SFRD predicted from simulations, especially towards high redshifts. This uncertainty is currently unavoidable due to the poor understanding of feedback effects and the large range of halo masses contributing to the SFRD. The fitting parameters shown in Table 1 and used in equation (8) underestimate the SFRD at $z > 1$ compared to other observationally based models, such as the ones by Hopkins & Beacom (2006) (hereafter, HB+06), Behroozi, Wechsler & Conroy (2013) (hereafter, Be+13), or Madau & Dickinson (2014) (hereafter, MD+14). These models are fits of the SFRD estimated using different sets of observational data in the infrared, optical, radio, and *UV* bands. We compare between these models predictions and the SFRD derived from Hα measurements to illustrate how different probes of incomplete data samples at high-z lead

Downloaded from https://academic.oup.com/mnras/article-abstract/475/2/1587/4768282 by University of Groningen user on 20 March 2019

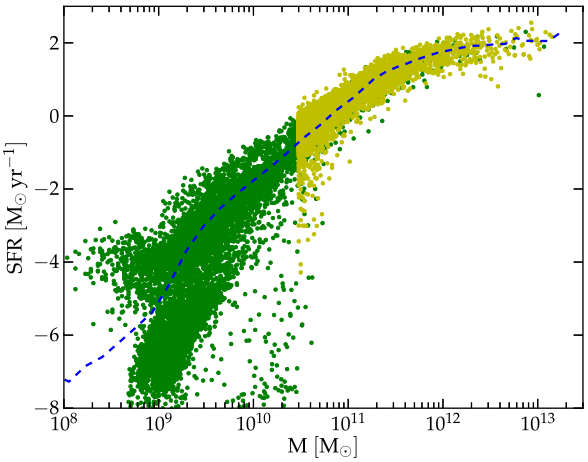

Figure 2. SFR as a function of halo mass at $z \sim 2.2$ from the Guo et al. (2013) galaxy catalogue. The dashed line marks the average in this relation. The yellow and green dots correspond, respectively, to DM haloes extracted from the Millennium and Millennium II cosmological dark matter simulations.

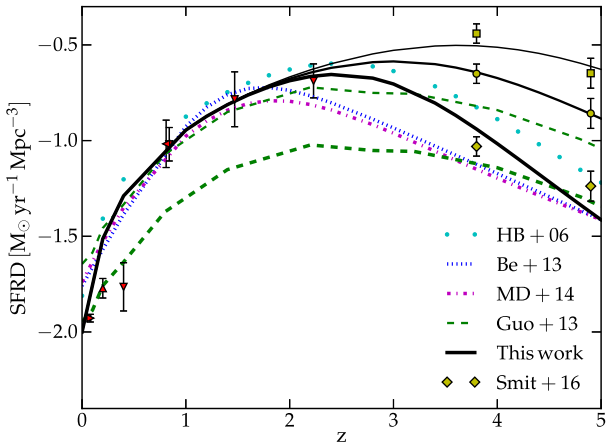

Figure 3. Cosmic SFRD as a function of redshift according to several models. The Guo et al. (2013) SFRD is shown for the default efficiency of conversion of gas into stars of $\epsilon = 0.2$ (green thick dashed line) and also for $\epsilon = 0.4$ (green thin dashed line). The symbols correspond to observational constraints based on H α emitters. The red triangles are derived from H α LFs at $z = 0.08$ (Ly et al. 2007), at $z = 0.0225$ (Gallego et al. 1995), at $z = (0.4, 0.84, 1.47, 2.23)$ (Sobral et al. 2013), at $z = 0.81$ (Sobral et al. 2015), and at $z = 0.2$ (Stroe & Sobral 2015). The yellow symbols correspond to SFRD constraints, derived from observed H α fluxes and UV continuum luminosities (Smit et al. 2016). These symbols assume different values for the extinction suffered by H α emission. Squares, circles, and diamonds correspond, respectively, to $A_{\mathrm{H}\alpha} = 1.0$, $A_{\mathrm{H}\alpha} = 0.45$, and $A_{\mathrm{H}\alpha} = 0.03$. The latter value was obtained assuming an SMC extinction law.

to a large uncertainty in the cosmic SFRD evolution. For a Salpeter IMF and for the conversion factor between UV luminosity and SFR shown in equation (1), the HB+06 SFRD is

$$\mathrm{SFRD}(z) = \frac{h}{0.77}\,\frac{0.012 + 0.091z}{1 + (z/3.3)^{5.3}}\,\mathrm{M}_\odot\,\mathrm{yr}^{-1}\,\mathrm{Mpc}^{-3}, \tag{9}$$

whereas the Be+13 SFRD is

$$\mathrm{SFRD}(z) = \frac{0.311}{10^{-0.997(z-z_0)} + 10^{0.241(z-z_0)}}\,\mathrm{M}_\odot\,\mathrm{yr}^{-1}\,\mathrm{Mpc}^{-3}, \tag{10}$$

with $z_0 = 1.243$. Finally, the MD+14 SFRD is given by

$$\mathrm{SFRD}(z) = 0.015\frac{(1+z)^{2.7}}{1 + [(1+z)/2.9]^{5.6}}\,\mathrm{M}_\odot\,\mathrm{yr}^{-1}\,\mathrm{Mpc}^{-3}. \tag{11}$$

In Fig. 3 we show the SFRD evolution predicted by the referred models. This figure shows that none of these SFRD models provide a good fit to the star formation traced by H α emission.

We note that the high redshift points in Fig. 3 are derived from H α emitters, which show an excess H α flux compared to the measured UV fluxes. This might be due to dust correction uncertainties, a bursty or rising star formation history, the shape of the ionizing spectrum, or other reasons. For a further discussion on this subject, see Smit et al. (2016). As a result, at high z, the SFRs and SFRDs inferred from the H α flux using equation (3) might be overestimated. Nevertheless, we will start by ignoring this H α excess since its origin is not yet clear. In order to be consistent, we will use equation (3) to connect SFR and H α emission for the $z \sim$0–5 redshift range. In Sections 9 and A3, we will discuss the impact of this decision on our conclusions.

We fit the SFRD traced by H α emission by updating the parameters in the Cole et al. (2001) fitting function:

$$\mathrm{SFRD}(z) = \frac{0.01 + 0.1036z}{1 + (z/z_1)^e}\,\mathrm{M}_\odot\,\mathrm{yr}^{-1}\,\mathrm{Mpc}^{-3}, \tag{12}$$

where $z_1 = 4$ and $e = 5$. These parameters can be derived from the H α intensity given by equation (7), using the conversion factor between SFR and H α luminosity in equation (3). We assume a dust extinction of $A_{\mathrm{H}\alpha} = 1$ mag at low redshift ($z \lesssim 2.3$) and a lower extinction of $A_{\mathrm{H}\alpha} = 0.45$ mag at $z \sim 4 - 5$ (shown as the middle thickness black solid line in Fig. 3). The same fit for a constant H α extinction of $A_{\mathrm{H}\alpha} = 1$ mag can be obtained using $z_1 = 4.8$ and $e = 5.3$ (shown as the thin black solid line in Fig. 3). The SFRD formula for a Small Magellanic Cloud (SMC) extinction curve (Gordon et al. 2003) can be obtained with $z_1 = 3.25$ and $e = 5.9$ (shown as the thick black solid line in Fig. 3).

From the current H α observations, one can trace the LF and use it to derive the cosmic SFRD. However, in order to estimate the H α intensity power spectrum, we need to establish a relation between SFR and DM halo mass. Since we cannot observationally probe the masses of the DM haloes hosting the H α emitters, we adopt the SFR–halo mass relations described in Section 3.2.1. We normalize these relations to our observationally based SFRD fit given by equation (12) (with $z_1 = 4$ and $e = 5$) and adopt them as our base SFR model.

In the following sections, we use this SFR model to estimate the average H α flux originating from a DM halo, the H α bias, and finally the power spectra of H α intensity spatial fluctuations. Note that at low redshift there are a few observational points below our theoretical model. However, the adopted simple, yet physically based model cannot properly fit these points and the constraints at $z \sim 1$ at the same time.

3.2.3 *Power spectrum*

The total power spectrum of H α emission can be written as

$$P^{\mathrm{tot}}_{\mathrm{H}\alpha}(k, z) = P^{\mathrm{clus}}_{\mathrm{H}\alpha}(k, z) + P^{\mathrm{shot}}_{\mathrm{H}\alpha}(z), \tag{13}$$

where the first term accounts for the galaxy clustering and is given by:

$$P^{\mathrm{clus}}_{\mathrm{H}\alpha}(k, z) = \bar{b}^2_{\mathrm{H}\alpha}\,\bar{I}^2_{\mathrm{H}\alpha}\,P_{\delta\delta}(k, z), \tag{14}$$

Downloaded from https://academic.oup.com/mnras/article-abstract/475/2/1587/4768282 by University of Groningen user on 20 March 2019

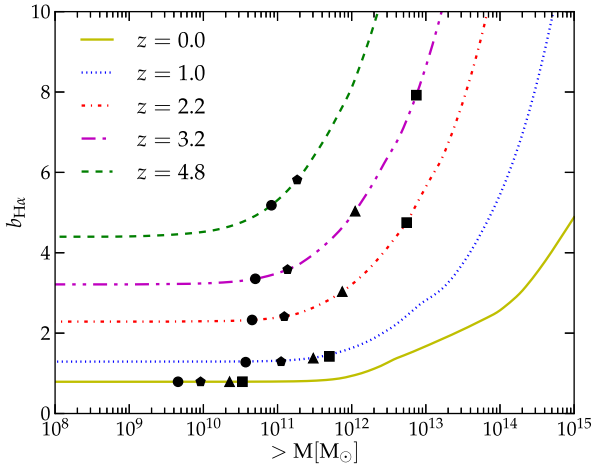

Figure 4. Cumulative bias of Hα emission. The x-axis corresponds to the minimum mass of a halo used on the bias integration. The circles, pentagons, triangles, and squares correspond, respectively, to flux limits of (10^{-18}, 10^{-17}, 1.2×10^{-16}, 3×10^{-16}) erg s^{-1} cm^{-2}.

where $b_{\rm H\alpha}$ is the bias between Hα emission and the matter power spectrum ($P_{\delta\delta}$). The Hα luminosity weighted bias is

$$\bar{b}_{\rm H\alpha}(z) \equiv \frac{\int_{M_{\rm min}}^{M_{\rm max}} {\rm d}M\, b(M,z)\, L_{\rm H\alpha}(M,z) \frac{{\rm d}n}{{\rm d}M}}{\int_{M_{\rm min}}^{M_{\rm max}} {\rm d}M\, L_{\rm H\alpha}(M,z) \frac{{\rm d}n}{{\rm d}M}}, \quad (15)$$

where $b(M, z)$ is the halo bias and ${\rm d}n/{\rm d}M$ is the DM halo mass function. The integration limits for the halo mass are $M_{\rm min} = 10^8$ M$_\odot$ and $M_{\rm max} = 10^{15}$ M$_\odot$. The clustering term dominates the observed line power spectrum at large scales, whereas on small scales it is dominated by the second term, namely the shot noise caused by the discrete distribution of galaxies (e.g. Visbal & Loeb 2010):

$$P_{\rm H\alpha}^{\rm shot}(z) = \int_{L_{\rm min}}^{L_{\rm max}} {\rm d}L \frac{{\rm d}n}{{\rm d}L} \left[\frac{L_{\rm gal}^{\rm H\alpha}}{4\pi D_{\rm L}^2} y(z) D_{\rm A}^2 \right]^2. \quad (16)$$

The relation between line luminosity and halo mass, used in equation (15), has a large scatter. Moreover, it is rarely possible to observationally probe DM halo masses. The bias of Hα emitters is observationally constrained at $z \sim 2.24$ to be $b_{\rm H\alpha} = 2.4^{+0.1}_{-0.2}$ (Geach et al. 2012).

This bias was derived by comparing a sample of 370 Hα emitters detected by HiZELS with predictions from GALFORM semi-analytic models (Cole et al. 2000). The HiZELS uniform complete sample contains emitters with luminosities down to $L_{\rm H\alpha} = 2 \times 10^{42}$ erg s^{-1}. However, the referred bias was estimated assuming a lower luminosity limit of $L_{\rm H\alpha}^{\rm min} = 10^{41}$ erg s^{-1}. Since the Hα bias decreases towards lower luminosities, the total Hα emission bias might be lower than the quoted value.

Given the lack of observational constraints for the full redshift range of interest, we estimate the Hα bias assuming that Hα emission scales with the galaxy SFR following equation (3). The cumulative Hα bias as a function of redshift is shown in Fig. 4 using our SFR model. This figure clearly shows that the current observational constraints (limited to high fluxes) cannot be used to calculate the bias for a wide range of galaxy luminosity, hence a theoretical model is needed.

The total Hα bias depends on the evolution of the slope of the relation between the SFR and the mass of a DM halo, but it is independent of the amplitude of this relation. Nonetheless, we use our normalized SFR-halo mass relation described in Sections 3.2.1 and 3.2.2, so that we can estimate the Hα bias as a function of minimum halo mass. This allows us to estimate the cumulative Hα bias according to several flux cuts, relevant for the upcoming Hα surveys.

At low redshifts and for large halo masses, each DM halo contains several galaxies. However, there is usually one galaxy dominating the SFR in the halo and so, for simplicity, we assume that the Hα flux in a halo corresponds to the emission from one galaxy.

4 SIMULATED Hα EMISSION FROM GALAXIES AND FROM THE IGM

Intensity mapping surveys will be sensitive to Hα emission from galaxies. However, these surveys will also detect Hα emission from the large-scale IGM filaments connecting the DM haloes in which galaxies reside. In this section, we use simulations to estimate the Hα emission from these two media and compare their relative contribution to the total Hα emission intensity and power spectrum.

4.1 The simulation

The intensity of IGM Hα emission scales non-linearly with the gas density and temperature. Therefore, we run a simulation code with a high spatial resolution in order to model the local properties of the gas. We start with a dark matter only run made with the parallel code Gadget 2 (Springel, Yoshida & White 2001; Springel 2005). This simulation covers a volume of (200 Mpc h^{-1})^3 with 1024^3 particles, each with a mass of 6.5×10^8 M$_\odot$ h^{-1}.

Simulation outputs in the redshift range ~0–5 are used to estimate the Hα intensity. In addition, outputs up to $z \sim 10$ are used to estimate the contamination by background lines in Hα intensity maps.

The particles are distributed in 3D boxes with 1200^3 cells following the cloud in cell method. In order to model the conditions of the IGM gas, we assume that the spatial distribution of the baryonic matter follows that of dark matter. The gas temperature, the neutral hydrogen number density ($n_{\rm H\,I}$), the ionized hydrogen number density ($n_{\rm H\,II}$), and the electron number density ($n_{\rm e}$) are estimated following the prescription outlined in Kooistra, Silva & Zaroubi (2017).

Additionally, the Amiga halo finder code (Gill, Knebe & Gibson 2004) is used to extract DM haloes from the Gadget 2 outputs. The minimum halo mass in our simulation is $M_{\rm min} = 6.5 \times 10^9$ M$_\odot$. To each of these haloes we attribute an SFR (normalized to our SFRD model) from a random halo with a similar mass from the Guo2013 galaxy catalogue. The Hα emission from the DM haloes is obtained with equation (3), assuming a dust extinction of $A_{\rm H\alpha} = 1$ mag. Fig. 5 shows a map of the total Hα emission from galaxies and from the IGM at redshift 2 (notice the logarithmic colour scale). This figure clearly shows that the contribution of the diffuse component is subdominant. The procedure used to derive the IGM Hα emission from the simulation is outlined in Section 4.2.

4.2 Hα IGM emission

At $z \sim 5$, the IGM gas is kept highly ionized by the ultraviolet background radiation (UVB) together with ionizing radiation from local sources. Most of this gas is located in a large scale filamentary structure connecting galaxies and galaxy clusters. The relative overdensity of filamentary gas allows for the existence of small clumps of neutral gas. Therefore, in these filaments, there will be

Downloaded from https://academic.oup.com/mnras/article-abstract/475/2/1587/4768282 by University of Groningen user on 20 March 2019

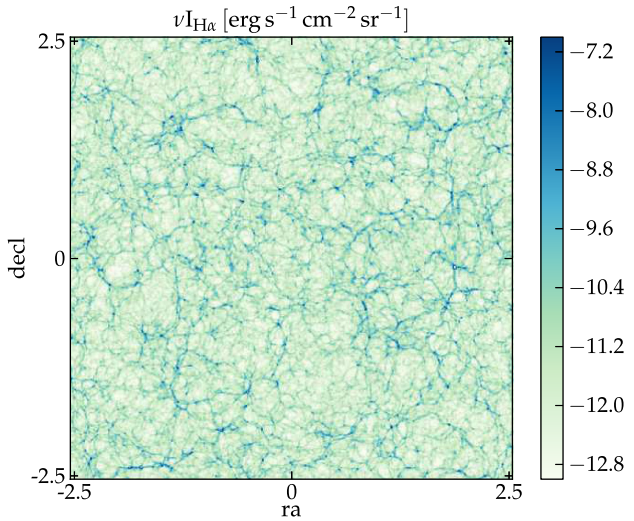

Figure 5. Map of H α emission from galaxies and from the IGM at $z \sim 2$. The map scale corresponds to $\log_{10}(\nu I_{H\alpha}[\mathrm{erg\,s^{-1}\,cm^{-2}\,sr^{-1}}])$.

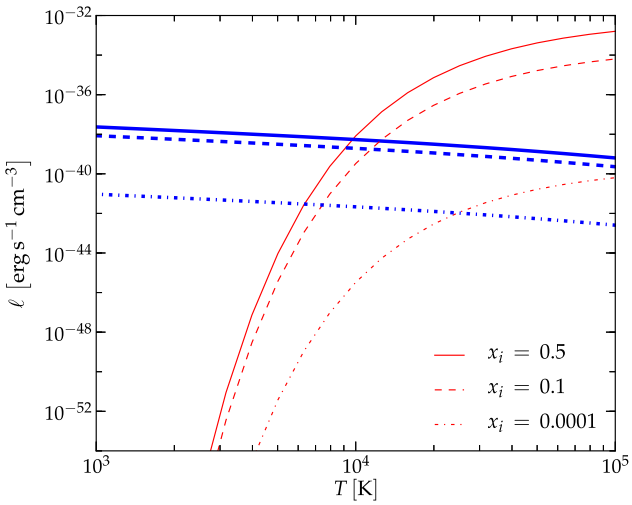

Figure 6. Luminosity density of H α emission from gas with a hydrogen density of $n_H = 10^{-6}\,\mathrm{cm^{-3}}$. Recombination H α emission (blue thick lines) and collisional excitation H α emission (red thin lines) are shown for gas with an ionized fraction of $x_i = (0.5, 0.1, 0.0001)$, for, respectively, the solid, dashed, and dot–dashed lines. Note that in the IGM the average hydrogen ionized fraction is very small, of the order of 10^{-5} at $z \sim 0$.

H α emission originating in hydrogen recombinations and collisional excitations. The luminosity density per comoving volume of H α emission from hydrogen recombinations in the IGM is

$$\ell_{\rm rec}^{\rm IGM}(z) = f_{\rm rec}\,\dot{n}_{\rm rec}\,E_{\rm H\alpha}, \tag{17}$$

where $E_{\rm H\alpha} = 1.89\,\mathrm{eV}$ is the energy of an H α photon. $f_{\rm rec}$ is the probability of emission of an H α photon per recombination of a hydrogen atom. The value of $f_{\rm rec}$ at a gas temperature $T = 10^4$ K is 0.45 (Osterbrock & Ferland 2006). The number density of recombinations per second, $\dot{n}_{\rm rec}$, is:

$$\dot{n}_{\rm rec}(z) = \alpha_B(T)\,n_e(z)\,n_{\rm H\,II}(z). \tag{18}$$

Here $\alpha_{\rm B}$ is the case B recombination coefficient for hydrogen. The gas temperature in the IGM can be much lower than that of the ISM. Therefore, we also consider a temperature-dependent effective recombination coefficient for the H α emission, $\alpha_{\rm B}^{\rm H\alpha}(T) = f_{\rm rec}(T)\,\alpha_{\rm B}(T)$. We take the fitting formula from Raga et al. (2015), hereafter Raga+15:

$$\alpha_{\rm B}^{\rm H\alpha} = \frac{4.85\times10^{-23}}{T^{0.568} + 3.85\times10^{-5}T^{1.5}}\,\mathrm{cm^3\,s^{-1}}. \tag{19}$$

This fit follows the same trend as the tabulated values from Osterbrock & Ferland (2006). The H α luminosity due to collisional excitations is

$$\ell_{\rm coll}^{\rm IGM} = E_{\rm H\alpha}\,n_{\rm e}\,n_{\rm H\,I}\,q_{\rm eff}^{\rm H\alpha}, \tag{20}$$

where $n_{\rm H\,I}$ is the neutral hydrogen number density. The parameter $q_{\rm eff}^{\rm H\alpha}$ is the effective collisional excitation coefficient for H α emission, which is taken from Raga+15 as

$$q_{\rm eff}^{\rm H\alpha} = \frac{3.57\times10^{-17}}{T^{0.5}}e^{-140360/T}\left(1 + \frac{7.8}{1+5\times10^5/T}\right). \tag{21}$$

The relative importance of recombination and collisional excitation for H α emission is illustrated in Fig. 6. The plotted luminosity densities assume hydrogen number densities of $n_{\rm H} = 10^{-6}\,\mathrm{cm^{-3}}$, $n_{\rm H\,II} = n_{\rm e} = x_i n_{\rm H}$, and $n_{\rm H\,I} = (1 - x_i)n_{\rm H}$, where x_i is the gas ionized fraction. As a reference, the average hydrogen number density in the IGM is about $n_{\rm H} = 1.9\times10^{-7}\mathrm{cm^{-3}}$. The assumed ionized fractions of the gas are presented in the figure. The gas temperature and its ionization state are both positively correlated with the strength of the extragalactic background radiation. The assumption of thermal and ionization equilibrium sets the H I gas temperature to $T \sim 10^4$ K. Hence, recombinational emission is the dominant process for generating H α photons in this medium.

The intensity of H α emission from the IGM is

$$I_{\rm H\alpha}^{\rm IGM}(z) = \frac{\left(\ell_{\rm rec}^{\rm IGM} + \ell_{\rm coll}^{\rm IGM}\right)\,D_A^2}{4\pi D_L^2}\,y(z). \tag{22}$$

Using this equation, we estimate the H α intensity for each cell of our simulation boxes. Cells with densities above the threshold for collapse, which at $z \sim 0$ is $\Delta_{\rm c} \sim 328$, should contain galaxies. These galaxies will contain most of the baryonic mass in the cell. The remaining baryonic mass will be highly heated and ionized by the local sources. Therefore, we assume that the H α IGM emission in these regions is zero.

Fig. 7 shows the redshift evolution of the simulated H α intensity from the IGM and from galaxies. The considered model results in galaxy H α emission dominating over H α emission from the IGM. This figure also shows that, after masking the emission from galaxies with H α fluxes above $10^{-18}\,\mathrm{erg\,s^{-1}\,cm^{-2}}$, the remaining signal is still dominated by emission from low-luminosity galaxies and not from IGM emission. At $z \sim 0$, the intensities of these two faint sources are similar due to the low redshift emission being highly dominated by bright sources.

4.3 H α emission power spectra

Power spectrum analysis is the most common statistic with which intensity maps are studied. Fig. 8 shows the power spectra of simulated H α emission from galaxies at different redshifts. The theoretical H α power spectrum is also presented in this figure in order to show this line power at large scales. The power spectra in Fig. 8 correspond to emission from galaxies in DM haloes with masses above $6.5\times10^9\,\mathrm{M_\odot}$. Our theoretical estimates indicate that even at $z \sim 5$, where the emission from low mass haloes is more important, their relative contribution to the total H α intensity is of the order of 5 per cent. Therefore, there should be no meaningful loss

Downloaded from https://academic.oup.com/mnras/article-abstract/475/2/1587/4768282 by University of Groningen user on 20 March 2019

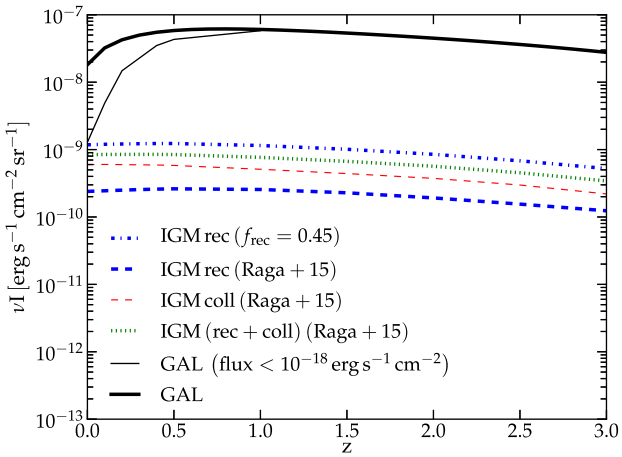

Figure 7. Intensity of Hα emission from galaxies (two top lines) and from the IGM (bottom lines). The black thin solid line accounts for the emission from galaxies with Hα fluxes flux $<10^{-18}$ erg s^{-1} cm^{-2}. The blue dashed-dotted line assumes $f_{rec} = 0.45$, while the red lines assume the temperature-dependent Hα emission rates from Raga+15.

in power due to the lack of emission from lower mass haloes in our simulations.

The IGM Hα emission is characterized by a small bias (from our simulations we obtain $b_{H\alpha}^{IGM} \sim 1$, consistent with most of the emission originating in low-density gas). Given the low intensity of the IGM emission, its power spectrum amplitude is much smaller than that of galaxy emission. We, therefore, do not show the IGM power spectrum in Fig. 8.

5 SURVEYS OF Hα EMISSION

Here we make predictions for four instruments: *Euclid* and *WFIRST* that will measure Hα emission from resolved galaxies, and SPHEREx and CDIM that will operate as Hα intensity mapping probes. The properties of the spectroscopic surveys of these instruments are listed in Table 2.

Euclid is a space mission under development by the European Space Agency that should start observing galaxies in 2020. *WFIRST* is a competing experiment being developed by NASA. It is projected to be launched also in 2020. In addition to their spectroscopic capabilities, the two satellites will carry out photometric surveys that will cover slightly higher frequency/redshift ranges than their spectroscopic surveys. More importantly, the photometric surveys will allow us to probe galaxies much deeper in magnitude. *Euclid* will reach ∼24 mag in 5σ detections of point sources using three filters (Y, J, and H) and *WFIRST* will reach close to 26.5 mag using four filters (Y, J, H, and $F184$). The frequency resolution of these photometric surveys is enough to probe and constrain cosmology using the BAO scale. However, due to the short time-scales associated with the astrophysical processes at hand, Hα emission is better constrained using the spectroscopic surveys of these satellites.

The SPHEREx instrument is meant to be used as an explorer and so it has a broad range of science goals spanning from cosmic inflation via non-Gaussianity to galaxy evolution and Galactic ices (Doré et al. 2016). On the other hand, the CDIM instrument is a NASA Probe that focuses on greatly improving our knowledge of galaxy formation and evolution. This mission's main objective is to probe galaxies and IGM emission during the Epoch of Reionization. The SPHEREx mission is at an advanced stage of formulation and was selected for a Medium-Class Explorers Mission concept study by NASA in 2017. It will be a shallow all-sky survey but with deep imaging data collected in the ecliptic poles, where the poles are imaged at every orbital pass. In this study we will only consider the SPHEREx deep survey since its field of view is wide enough to constrain Hα emission. CDIM remains a concept study and its exact survey strategy as well as final details are yet to be determined.

Intensity mapping survey data consist of three-dimensional intensity maps, where each observational voxel is set by a certain angular resolution and covers a wide range of frequency. Given the large volume covered by each observed voxel, it will contain emission from several unresolved sources. Instead of resolving galaxies, IM surveys aim at detecting the overall emission from both bright and faint sources, as well as extended emission sources. SPHEREx and CDIM plan to detect Hα emission in IM mode in order to be unconstrained by flux limits and therefore probe the full signal. In these surveys, the recovery of the target signal, i.e. the intensity and spatial fluctuations of Hα emission, is usually done through power spectrum analysis. However, the same instruments can also operate as galaxy surveyors. As such, they will characterize the galaxies down to the flux limit listed in Table 2. In this case, due to time limitations, SPHEREx and CDIM will observe over smaller areas.

IM surveys are a better choice for cosmological purposes since they can cover large volumes in a short time. On the other hand, in traditional galaxy survey mode, SPHEREx and CDIM instruments will be able to map bright interloping lines. Furthermore, in the case where the foreground removal strategies in intensity maps are not successful, these instruments will still be able to use the signal from resolved galaxies for astrophysical purposes.

The large resolving power of galaxy surveys will allow them to provide detailed information on the emission from different galaxy populations. The *Euclid* and *WFIRST* galaxy surveys will probe the Hα LF. On the other hand, SPHEREx and CDIM IM surveys will

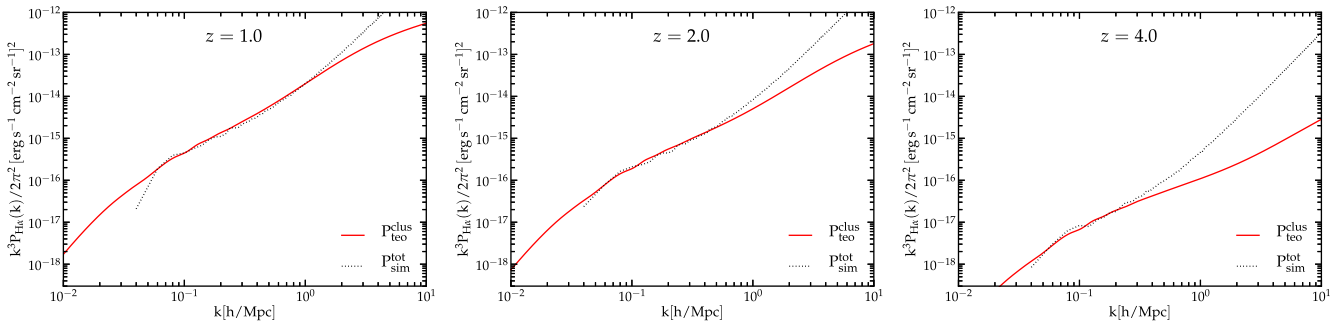

Figure 8. Simulated power spectra of Hα emission from galaxies as it will be observed by the IM surveys (black dashed lines). The solid lines show the theoretical clustering power spectrum associated with each survey.

Downloaded from https://academic.oup.com/mnras/article-abstract/475/2/1587/4768282 by University of Groningen user on 20 March 2019

Table 2. Parameters for the spectroscopic surveys.

Instrument	λ (μm)	$z_{\mathrm{H}\alpha}$	δ_θ (arcsec)	R	Flux limit (erg s^{-1} cm^{-2})	FOV total (deg^2)
SPHEREx deep	0.75–4.18	0.1428–5.369	6.2	41.4	10^{-17}	200
SPHEREx deep	4.18–5.0	5.369–6.6187	6.2	135	10^{-17}	200
CDIM deep	0.75–7.5	0.14–10.43	1	500	$\leq 4 \times 10^{-18}$	25
CDIM	0.75–7.5	0.14–10.43	1	500	10^{-17}	300
Euclid deep	1.1–2.0	0.68–2.036	0.3	250	3×10^{-16}	40
WFIRST	1.35–1.95	1.05–1.96	0.15	75	1.2×10^{-16}	2227

provide measurements of the integrated H α intensity. Therefore, IM surveys will probe the entire galaxy population and suffer a lot less from selection biases than galaxy surveys. An additional advantage of IM surveys is that the redshift of the source of emission is obtained automatically. This makes them particularly useful for probing the time evolution of global galaxy properties. Moreover, given the large frequency range spanned by the SPHEREx and CDIM surveys, they will be able to target several emission lines and to probe galaxy emission at higher redshifts than *Euclid* and *WFIRST*. In particular, the CDIM surveys will cover the high frequencies corresponding to Ly α emission from the EoR. CDIM also has the advantage of having a frequency resolution that makes it possible to separate between emission in the H α line and in the nearby N II doublet lines.

The potential of each type of instrument to probe galaxies H α emission and to constrain different galaxy properties as well as their redshift evolution is described in detail in Appendix A.

6 CONTAMINATION IN H α OBSERVATIONS

In both galaxy surveys and IM surveys, observations of H α emission will be contaminated by emission from interloping lines. This contamination needs to be identified, evaluated, and, if necessary and possible, removed.

*Euclid*and *WFIRST* low-resolution spectra will be fitted with galaxy SED templates, which can, in case the signal to noise ratio is high, be used to identify the observed line. This will, however, not always be possible due to the narrow frequency range covered by these instruments' filters. Also, the lack of information on the redshift of the source might result in line confusion. Moreover, neither of these two surveys has enough frequency resolution to separate the peak of the H α line from that of the N II line doublet. Nevertheless, the bright galaxies detected by these surveys are important to constrain the physical properties of the H α emitters. These galaxies will also be useful to determine the role of the environment in the extinction suffered by H α emitters.

Line contamination is also a problem for IM surveys, given that they are intrinsically characterized by detecting emission from all types of unresolved sources. The amount of contribution from line contaminants depends on the target line and on the observed frequency. Therefore, it has to be evaluated according to the frequency range covered by the survey. In the case that this contamination is higher than or comparable to the signal from the target line, part of it needs to be removed (masked) from the observational maps. Generally speaking, the H α intensity maps will be contaminated by several strong interloping lines, hence, their contamination needs to be accounted for. The observational voxel size will determine the percentage of voxels that need to be masked in order to efficiently reduce the contamination in the maps. In the case where a high portion of the voxels is masked ($\gtrsim$10 per cent), the recovery of the target signal might require a correction for the loss of flux in the target line. Therefore, the appropriate contamination removal strategy for an intensity mapping study is highly dependent on the survey properties.

In Subsection 6.1 we model the intensity and dust extinction suffered by each of the line contaminants. For the estimation of the observed intensity, we take into account that galaxy surveys will mainly observe bright systems, whereas IM surveys are expected to observe the total galaxy population. We continue by estimating the power spectra of line contamination, which is relevant for IM surveys (Subsection 6.2). We find that the contamination power spectrum is of the same order as that of the signal. Using simulations, we determine the masking fractions required to reduce the contamination power spectra to a level well below the predicted H α signal. We also present estimates of the masking fractions associated with increasing flux cuts (Subsection 6.3). We assume that the voxels that need to be masked, corresponding to bright foreground emission, will be identified independently by a galaxy survey. In the case of the SPHEREx and CDIM missions, the foregrounds survey can be performed by the same instrument operating in a different mode.

Additionally, intensity maps will suffer from continuum emission originating in the stellar and AGN continuum, as well as free–free, free–bound, two-photon emission and dust emission in the ISM. At the frequency range relevant for H α IM, this continuum contamination is dominated by stellar emission, since AGN emission only dominates the extragalactic continuum background at higher frequencies/energies (Silva et al. 2016). Continuum emission is expected to vary more smoothly with frequency compared to the signal from emission lines, which should quickly fluctuate in the frequency direction (Alonso et al. 2015). This smoothness is used in IM studies to fit and remove the continuum emission. Therefore, we assume that continuum emission can easily be fitted out of these maps and focus only on line contamination. The case for galactic contamination is similar, since these foregrounds are fitted in frequency and removed in the same way as extragalactic continuum foregrounds.

6.1 Observed intensity of line contaminants

In H α intensity maps, at $z < 5.0$, the main contaminants include the ionized oxygen [O II] 372.7 nm and [O III] 500.7 nm lines, and the hydrogen H β 486.1 nm and Ly α 121.6 nm lines. We also consider the contamination by the [N II] 658.3 nm/654.8 nm and [S II] 671.7 nm/673.1 nm doublet lines.

Table 3 presents a list of the contaminating lines and the redshifts from which they originate, in comparison to the redshift of the H α line. Given the very small frequency separation, the N II doublet lines originate from approximately the same redshift as the H α line and so they are not included in this table.

Downloaded from https://academic.oup.com/mnras/article-abstract/475/2/1587/4768282 by University of Groningen user on 20 March 2019

Table 3. Contaminant background lines in Hα intensity maps.

Line	λ_0 (nm)	$z(\lambda = 656.28$ nm)	$z(\lambda = 721.91$ nm)	$z(\lambda = 1181.30$ nm)	$z(\lambda = 1968.84$ nm)	$z(\lambda = 2625.12$ nm)	$z(\lambda = 3937.68$ nm)
Hα	656.28	0.00	0.20	0.80	2.00	3.00	5.00
S II	671.7	–	0.07	0.76	1.93	2.91	4.86
O III	500.7	0.31	0.57	1.36	2.93	4.24	6.86
Hβ	486.1	0.35	0.62	1.43	3.05	4.40	7.10
O II	372.7	0.76	1.13	2.17	4.28	6.04	9.57
Lyα	121.6	4.40	5.48	8.71	15.19	20.59	31.38

In order to model the contamination by each interloping line, we take the published relations between line luminosity and SFR and then compare/adjust them to the existing LF constraints, when possible. The intensity of these contaminating lines can be calculated by integrating over the SFR or the line LF, in the same way as was done for the Hα line, using equation (6).

In most cases, the intensity of the interloping lines is only constrained at low redshifts and the extrapolation of their LFs to higher redshifts is uncertain. The several factors involved in the line LF redshift evolution include the expected decrease in galaxy metallicity, the lower ionization state of the ISM gas, the possibility of the existence of low-density canals which would affect the galaxy extinction rates independent of the galaxy dust content, and others.

We now explore the contamination from each line in further detail.

N II contamination The relative contribution from the N II doublet to the Hα plus N II lines scales with the equivalent width (EW) of this peak and is usually in the range 10 per cent–50 per cent (Sobral et al. 2009, 2012). As a reference, the average value of the N II line contribution at $z = 1.47 \pm 0.02$ and for Hα fluxes above 7×10^{-17} erg s^{-1} cm^{-2} is ~22 per cent of the sum of the Hα and the N II line intensities (Sobral et al. 2012).

For galaxy surveys, we assume that the N II line contamination can be estimated from the Hα EW following the relation observed in SDSS galaxies and parametrized by Sobral et al. (2012) as:

$$\log([\mathrm{N\,II}]/\mathrm{H}\alpha) = -0.924 + 4.802E - 8.892E^2 + 6.701E^3 - 2.27E^4 + 0.279E^5, \quad (23)$$

where $E = \log[\mathrm{EW}_0(\mathrm{N\,II} + \mathrm{H}\alpha)]$.

However, IM surveys do not resolve individual galaxies. Therefore, this parametrization is impossible to apply. Given that, in intensity maps, each voxel contains emission from several galaxies, our default assumption is that the N II line contributes 22 per cent of the sum of the Hα and N II line intensities. A similar N II line contribution is predicted by Galaxy Evolutionary Synthesis (GALEV) models for galaxies with solar metallicities (Anders & Fritze-v. Alvensleben 2003). For sub-solar metallicities the N II contribution to the N II plus Hα line intensities should be smaller. One of the main advantages of the CDIM surveys is that they will have sufficient frequency resolution to distinguish between the Hα line emission and the N II line doublet emission.

From the surveys we consider in this work, only CDIM will have enough frequency resolution to do this. It should be noted that the evolution of the N II/Hα at $z \gtrsim 1.47$ is uncertain, due to lack of observations. Therefore, the assumption that this ratio is fixed will add a large systematic error to the estimation of the Hα signal. For further discussion on this topic, see Appendix A2.

S II contamination Most surveys also do not have good enough frequency resolution to separate the peak of the Hα line from that of the S II line doublet. Therefore, one needs to estimate the average contribution of this doublet line, using the same method we applied to the N II line.

The strength of the S II doublet has been found to vary between ~10 and 60 per cent of the Hα emission in SDSS star-forming galaxies (Kewley et al. 2006). However, in most cases the contribution of the S II lines to the (Hα + N II + S II) peak is ~12 per cent. This value is taken from Mármol-Queraltó et al. (2016), who evaluated it using Hα selected galaxies in the redshift range $1.23 \lesssim z \lesssim 1.49$ and with an average EW of 175 ± 14 Å.

The contribution from these doublet lines should be estimated directly from the survey data. Whenever that is not possible, we assume that the S II doublet line intensity is of the order of 12 per cent of the Hα + N II+ S II line intensity. We note that GALEV models for galaxies with solar metallicities predict that the S II line intensity corresponds to 9 per cent of the total Hα + N II + S II line flux (Anders & Fritze-v. Alvensleben 2003).

Hβ contamination We estimate the Hβ intrinsic luminosity from equation (3) and the recombination emission line ratios, which yields,

$$L^{\mathrm{int}}_{\mathrm{H}\beta}\,(\mathrm{erg\,s^{-1}}) = 4.43 \times 10^{40}\,\mathrm{SFR}\,(\mathrm{M_\odot\,yr^{-1}}). \quad (24)$$

Based on the Calzetti et al. (2000) extinction curve and the dust attenuation by OB galaxies in the COSMOS survey up to $z \sim 6.5$ (Scoville et al. 2015), the extinction suffered by the Hβ line is of the order of $A_{\mathrm{H}\beta} = 1.35 \times A_{\mathrm{H}\alpha}$. We use this the average Hβ intensity.

O II contamination The O II line luminosity can be estimated from the galaxy SFR using existing fits to the observational data. As a reference, we use the relation from Kennicutt (1998a) based on a ratio of 0.57 between the O II and Hα fluxes observed in local galaxies:

$$L_{\mathrm{O\,II}}\,(\mathrm{erg\,s^{-1}}) = (7.18 \pm 2.2) \times 10^{40}\,\mathrm{SFR}\,(\mathrm{M_\odot\,yr^{-1}}). \quad (25)$$

In Fig. 9, we compare the O II intensities predicted by SFRD-based models with observational constraints from the UKIDSS (Drake et al. 2013) and HiZELS (Khostovan et al. 2015) surveys. At low z, the theoretical curves are systematically above the predictions from Drake et al. (2013). However, at $z \sim 1.5 - 2$ our predictions fit quite well. As indicated by the more recent measurements from Matthee et al. (2017), this reflects a lower O II/Hα ratio at low z. The evolution of this ratio can be due to an increasing dust extinction at high z. It can also simply be due to technical issues with observations in the local Universe given that the surveys only measure the central kpc region of the galaxies (Matthee et al. 2017).

The high end of the O II LF is observationally probed up to a redshift of $z \sim 5$. However, this line intensity is only well constrained up to $z \sim 1.5$ (Khostovan et al. 2015). Recent observational constraints, reaching $z \sim 4.5$, predict this line EW to increase up to $z \sim 3.5$ and then to decline as a result of a higher ionization state of the ISM (Khostovan et al. 2016).

Downloaded from https://academic.oup.com/mnras/article-abstract/475/2/1587/4768282 by University of Groningen user on 20 March 2019

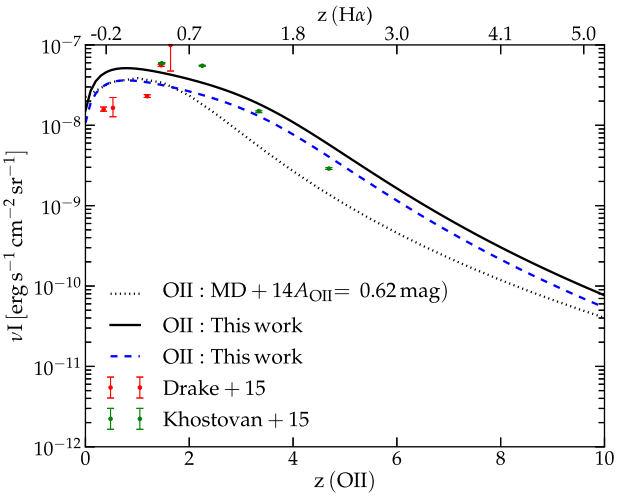

Figure 9. Intensity of observed O II line emission as a function of redshift. The lines show the O II intensity derived from our SFRD model (solid line and dashed line) and from the MD+14 SFRD model (dotted line). The solid and dotted black lines were corrected for a dust extinction of $A_{\rm O\,II} = 0.62$ mag, while the blue dashed line was corrected for a dust extinction of $A_{\rm O\,II} = 1.0$ mag. The dots correspond to observational points from UKIDSS (Drake et al. 2013) and HiZELS (Khostovan et al. 2015).

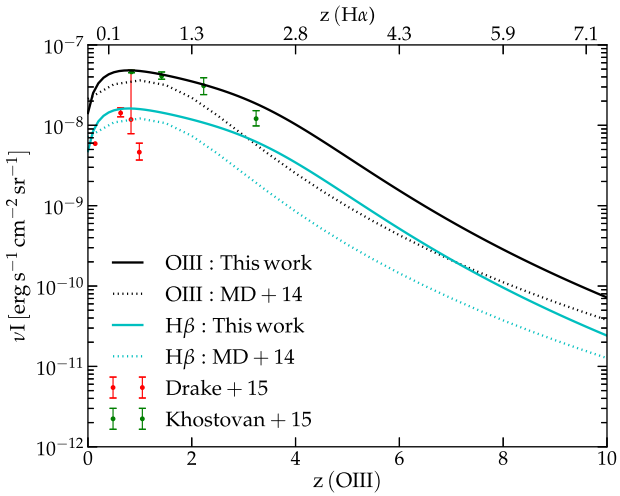

Figure 10. Intensity of observed O III line emission as a function of redshift. The black solid and black dotted lines show, respectively, the O III intensity derived from our SFRD model and from the MD+14 SFRD model. To the intrinsic line intensities, we applied a dust extinction of $A_{\rm O\,III} = 1.35$ mag. The dots correspond to observational points from the UKIDSS Ultra Deep Survey Field (Drake et al. 2013) and from HiZELS (Khostovan et al. 2015). Also shown in the cyan lines is the H β intensity obtained using equation (24), to which we applied a dust extinction of $A_{\rm H\,\beta} = 1.35$ mag. The cyan solid line assumes our SDRD model, while the cyan dotted line uses the MD+14 SFRD model.

The O II intensity in this figure assumes a low dust extinction of $A_{\rm O\,II} = 0.62$ mag (Hayashi et al. 2013). This is the average dust extinction of the observed O II emitting galaxies. However, the relevant extinction for IM studies should be that of the full galaxy population, which should be closer to $A_{\rm O\,II} = 1$ mag; see discussion in Hayashi et al. (2013).

O III contamination Similarly, the O III line luminosity can be estimated from the galaxy SFR, using existing fits to observational data. We take the relation from Ly et al. (2007), based on observations in the $z \sim 0.07 - 1.47$ redshift range and given by:

$$L_{\rm O\,III}\,({\rm erg\,s^{-1}}) = (1.32 \pm 2.7) \times 10^{41}\,{\rm SFR}\,({\rm M_\odot\,yr^{-1}}). \quad (26)$$

In Fig. 10, we compare the O III intensities predicted by SFRD-based models with observational constraints from the UKIDSS (Drake et al. 2013) and HiZELS (Khostovan et al. 2015) surveys. To the O III and H β line intensities, we applied a dust extinction of $A_{\rm O\,III} = A_{\rm H\beta} = 1.35$ mag, which corresponds to $A_{\rm H\,\alpha} = 1$ mag (Khostovan et al. 2015). As in the case of the O II line, our theoretical O III line curves fit better with observational LFs at $z \gtrsim 1.5$. We note, however, that the observational line ratios O III/O II and O III/H β are larger in high z galaxies (Castellano et al. 2017). Also, the EW of the O III line should increase towards galaxies with small stellar masses. Therefore, these high EWs are increasingly important towards high z, where galaxies are on average smaller (Khostovan et al. 2016). This indicates that the ISM in high z galaxies is characterized by a higher ionization parameter than that of low z galaxies.

With the few currently available observations, it is still unclear whether these differences are due to redshift evolution of the ratios between lines, dust extinction, or technical differences in observations, such as aperture effects (Matthee et al. 2017). None the less, in the redshift range important for this study, predictions based on observations fit well with those from our SFRD-based model. Therefore, we estimate the contamination by O III line emitters using the latter model.

Ly α contamination Ly α from high redshift galaxies, $z > 4.4$, contaminates H α line observations in the redshift range $z \sim 0 - 5$. We take the Ly α LFs at $z \sim 5.7$ and $z \sim 6.6$ from Santos, Sobral & Matthee (2016), and integrate them down to $L_{\rm Ly\,\alpha} = 10^{38}\,{\rm erg\,s^{-1}}$. For the different possible values of the low-luminosity slope of the Ly α LF, the observed line intensity is between $(0.13 - 3.9) \times 10^{-8}\,{\rm erg\,s^{-1}\,sr^{-1}\,cm^{-3}}$ at $z = 5.7$ and between $(0.036 - 1.1) \times 10^{-8}\,{\rm erg\,s^{-1}\,sr^{-1}\,cm^{-3}}$ at $z = 6.6$. This high uncertainty is due to, at these redshifts, the Ly α LF only being observationally constrained down to a luminosity of $\sim 10^{42.5}\,{\rm erg\,s^{-1}}$.

The Ly α intensity can also be estimated from the SFR as

$$L_{\rm Ly\alpha}\,({\rm erg\,s^{-1}}) = 1.1 \times 10^{42}\,{\rm SFR}\,({\rm M_\odot\,yr^{-1}}). \quad (27)$$

This observational relation was obtained using galaxies in the local Universe (Kennicutt 1998a).

Using our SFR model the Ly α line intrinsic intensity is then $6 \times 10^{-8}\,{\rm erg\,s^{-1}\,sr^{-1}\,cm^{-3}}$ at $z = 5.7$ and $2.6 \times 10^{-8}\,{\rm erg\,s^{-1}\,sr^{-1}\,cm^{-3}}$ at $z = 6.6$.

The observed line intensity was obtained by correcting the Ly α line intensity for the average of the Ly α photon escape fraction ($f_{\rm esc}^{\rm Ly\alpha}$). Due to the lack of good observational, for the Ly α dust extinction in galaxies, we take $f_{\rm esc}^{\rm Ly\alpha}$ from the high-resolution simulations of Yajima et al. (2014). As a reference this study predicts the average value of this escape fraction to be $f_{\rm esc}^{\rm Ly\alpha}(z = 5.5) \sim 0.5$.

The Ly α intensity estimated from LFs is smaller than that estimated using our SFR model. LFs are obtained using galaxy survey data which are unable to detect scattered Ly α photons around the galaxy. These photons will, however, be detectable by IM surveys. Therefore, we estimate this line contamination in intensity maps using our SFR estimate.

There will be additional contamination in the H α intensity maps from Ly α emission originating from recombinations, collisional excitations, and scattering of Lyman-n photons in the IGM (Silva et al. 2013; Comaschi & Ferrara 2016). Even for the higher estimates for this scattered emission obtained by Comaschi & Ferrara (2016), its power spectrum will be considerably below the signal from

Downloaded from https://academic.oup.com/mnras/article-abstract/475/2/1587/4768282 by University of Groningen user on 20 March 2019

galaxies. Moreover, the bias associated with the IGM emission is very close to unity, so in power spectrum analysis, these IGM contributions are not important. For simplicity, we, therefore, ignore these contributions to the Ly α power spectrum.

6.2 Power spectra of line contamination

Intensity maps can be analysed in several ways. However, given the low signal-to-noise ratio in the maps expected in many experiments, the signal will most likely be detected statistically. The most obvious statistic to use is the intensity power spectrum (see e.g. Pritchard & Loeb 2012).

The target line and the interloping lines are emitted from different redshifts and so their emission originates in different volumes. One needs to account for a volume conversion factor when estimating the contamination power spectra. We estimate the contamination by background lines in the observed H α power spectrum as a function of the perpendicular and parallel components of the wavevector k, using the Gong et al. (2014) formula, given by:

$$P_{\rm obs}(k_\perp, k_\parallel) = \left[P^{\rm clus}_{\rm line}(z_{\rm f}, k_{\rm f}) + P^{\rm shot}_{\rm line}(z_{\rm f}, k_{\rm f})\right] \times \left(\left[\frac{\chi(z_{\rm s})}{\chi(z_{\rm f})}\right]^2 \left[\frac{y(z_{\rm s})}{y(z_{\rm f})}\right]\right), \quad (28)$$

where the clustering power spectrum is

$$P^{\rm clus}_{\rm line}(z_{\rm f}, k_{\rm f}) = \bar{I}^2_{\rm f}(z_{\rm f}) b^2_{\rm f}(z_{\rm f}) P_{\delta\delta}(z_{\rm f}, k_{\rm f}). \quad (29)$$

The indexes s and f indicate the source, i.e. H α, or the foreground/background line redshifts, respectively. The parameter r corresponds to the comoving distance, while $|\vec{k}_{\rm f}| = \left[(r_{\rm s}/r_{\rm f})^2 k^2_\perp + (y_{\rm s}/y_{\rm f})^2 k^2_\parallel\right]^{1/2}$ is the three-dimensional k vector at the redshift of the foreground/background line. $P_{\delta\delta}$ is the matter power spectrum and $b_{\rm line}$ is the bias between the interloping line luminosity and the dark matter fluctuations. Finally, the shot noise power spectrum due to the discrete nature of galaxies is:

$$P^{\rm shot}_{\rm line}(z) = \int_{M_{\rm min}}^{M_{\rm max}} {\rm d}M \frac{{\rm d}n}{{\rm d}M} \left[\frac{L(M, z)}{4\pi D^2_{\rm L}} y(z) D^2_{\rm A}\right]^2. \quad (30)$$

Notice that the contaminants power spectrum shown in equation (28) experiences a scale-dependent shift, as well as amplitude modification. This change, due to contamination, will increase/decrease the measured power spectrum. In the scales measured by the IM surveys, the contamination by background lines will be attenuated relative to the H α power spectrum, whereas the foreground interloping lines will have the opposite effect. Therefore, most studies ignore the influence of background lines (see e.g. Gong et al. 2014; Fonseca et al. 2017). However, we show here, after a careful estimation, that some of the background lines cannot be ignored.

Left-hand panels in Fig. 11 show the power spectrum of the most important background lines that can be confused with the H α emission. The amplitude of the lines shown in this plot was calculated assuming a survey capable of detecting the full-line emission. This is a reasonable assumption for IM surveys. The matter power spectrum was theoretically estimated using the publicly available code CAMB (Lewis, Challinor & Lasenby 2000).

Fig. 11 clearly shows that the contamination power spectrum from background lines is of the order of the H α power spectrum. Therefore, it is clear that this contamination is not negligible and, hence, cannot be ignored. Namely, some of this background contamination needs to be removed from observational maps in order to accurately recover the signal from H α emission. We note that the amplitude of the Ly α line contamination power spectra is very small and can always be ignored. We show its values only in the top left-hand panel of Fig. 11, whereas, in the lower panels it is ignored because it is even smaller.

6.3 Contaminants masking fractions derived from simulations

We use the simulations described in Section 4 to estimate the flux cuts that we need to mask contaminant line emission, in order to efficiently reduce their power spectra. With the same simulations we calculate the percentage of observational voxels that need to be masked to achieve these flux cuts.

The right-hand panel of Fig. 11 shows the residual line contamination after masking the brightest background emitters from the observational maps. Note that these power spectra have a bit more power at small scales than the theoretical ones, given that our simulation does not have haloes below $M_{\rm min} = 6.5 \times 10^9\,{\rm M}_\odot$ and so we are overestimating the shot noise. The contamination in H α intensity maps is considerably reduced at $z \sim 0.2$ by masking voxels containing the signal from background emitters with fluxes above $1.2 \times 10^{-16}\,{\rm erg\,s^{-1}\,cm^{-2}}$. This would decrease the contamination power spectrum to about 5–25 per cent of its initial amplitude. Moreover, it would only require masking less than 1 per cent of the observational voxels, both for SPHEREx and for CDIM.

At $z \sim 0.8$, masking voxels contaminated by line fluxes above $1.2 \times 10^{-16}\,{\rm erg\,s^{-1}\,cm^{-2}}$ would only slightly decrease the signal from background lines. This would leave the line contamination in the observed maps at the level of 10–20 per cent of the total observed power spectrum. A flux cut of $5.0 \times 10^{-17}\,{\rm erg\,s^{-1}\,cm^{-2}}$ would be much more successful at reducing this contamination. However, it is very observationally challenging to individually detect all the galaxies responsible for this emission down to this low flux level.

At $z \sim 2.0$ and at a scale of $k \sim 0.1\,h^{-1}$ Mpc, the H α signal will be approximately 5 times higher than the background lines signal. Meaningfully decreasing this contamination (to about 50 per cent of its initial value) at small scales would also require the masking of contaminant lines with fluxes down to $\sim 5.0 \times 10^{-17}\,{\rm erg\,s^{-1}\,cm^{-2}}$ (see Fig. 11).

The percentage of voxels lost, assuming these flux cuts and the voxel size of the CDIM and SPHEREx surveys, is always at the 0.1–1 per cent level. O III emitters dominate the contamination in these maps. Therefore, detecting and masking only O III line contaminants would be observationally easier and would still result in a meaningful reduction of the contamination in H α intensity maps.

The quoted masking fractions will only decrease the H α intensity by less than 1 per cent. All these results were confirmed using our simulations.

An alternative masking procedure is the so-called blind masking in which the brightest pixels are masked assuming that they belong to foreground galaxies. However, this type of masking will not work in the presence of background line contaminants, since by doing so, a large fraction of the target line would also be inevitably masked. For the previously quoted flux cuts, the percentage of H α signal that would be erased is of the order of 40–85 per cent.

As a side note, contamination by interloping lines causes anisotropies in the angular power spectrum because the different lines originate at different redshifts. The angular power spectrum can, therefore, be used to test if the masking procedure was successful.

Downloaded from https://academic.oup.com/mnras/article-abstract/475/2/1587/4768282 by University of Groningen user on 20 March 2019

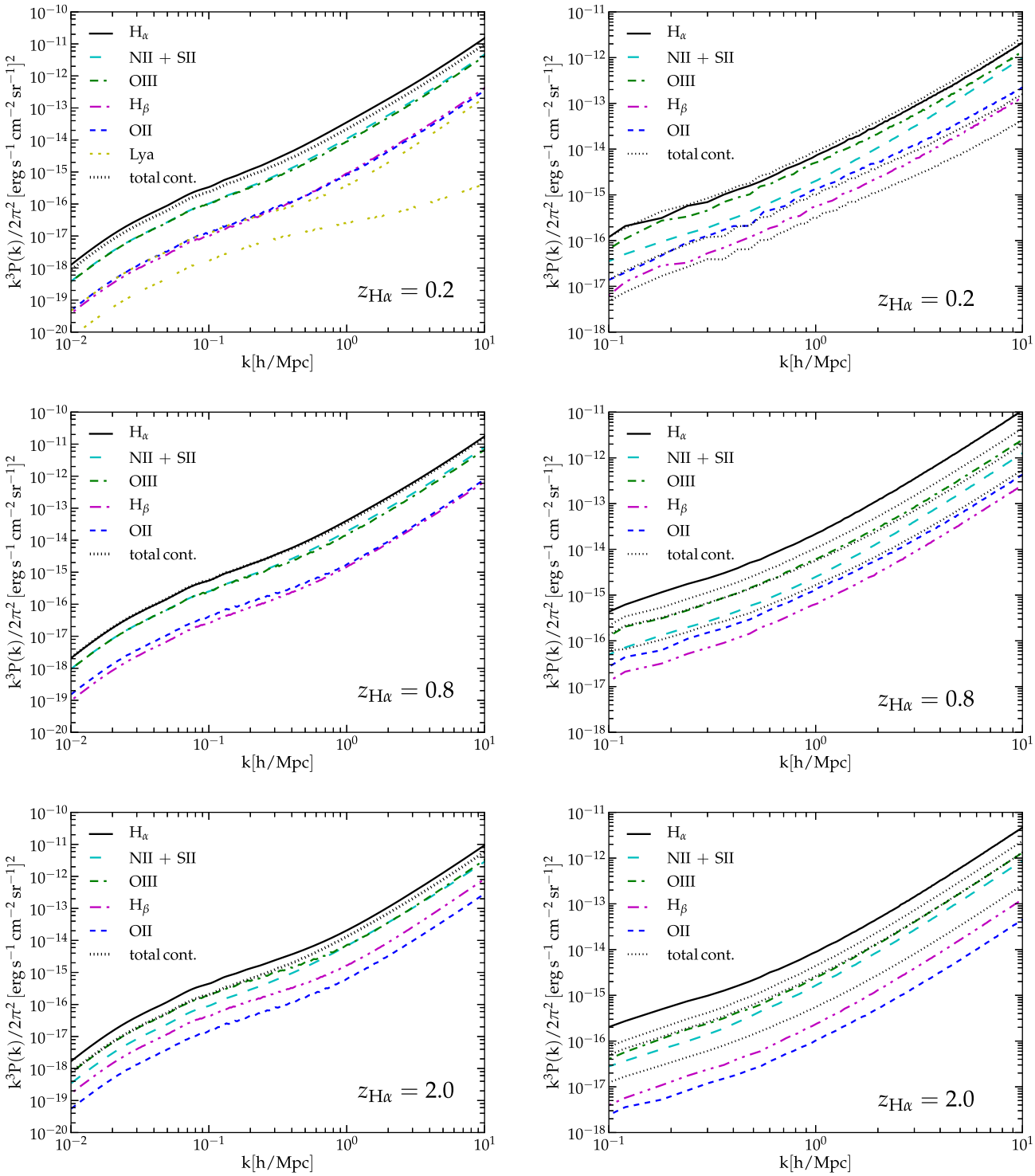

Figure 11. Left-hand panels: Theoretical power spectra of contamination by background lines in H α intensity maps at $z_{H\alpha} = 0.2, 0.8, 2.0$ (from top to bottom). The power spectra from the several interloping lines were scaled to the redshift of the H α line. The upper three dotted yellow line corresponds to Ly α emission from galaxies. The IGM Ly α emission power spectrum (bottom three dotted yellow line) was calculated using an intensity with double the value of the intensity from galaxies, a bias with the underlying density of one and no shot noise. Right-hand panels: Simulated power spectra of contamination by background lines in H α intensity maps at $z_{H\alpha} = 0.2, 0.8, 2.0$ (from top to bottom). These plots were obtained from our simulation and assume the cell resolution of the CDIM survey. The result would be very similar for a survey with the spatial and frequency resolution of SPHEREx. The top dotted line denotes the total contamination power spectrum (by the O III, O II, and H β lines), while the remaining dotted lines denote the contamination power spectra, after masking cells with fluxes in one of the foreground lines above a given threshold. For $z = 0.2$ and $z = 0.8$, the flux thresholds for masked cells are 1.2×10^{-16} erg s^{-1} cm^{-2} (middle dotted line) and 5.0×10^{-17} erg s^{-1} cm^{-2} (bottom dotted line). For $z = 2$ the flux thresholds for masked cells are 5.0×10^{-17} erg s^{-1} cm^{-2} (middle dotted line) and 1.0×10^{-17} erg s^{-1} cm^{-2} (bottom dotted line).

Downloaded from https://academic.oup.com/mnras/article-abstract/475/2/1587/4768282 by University of Groningen user on 20 March 2019

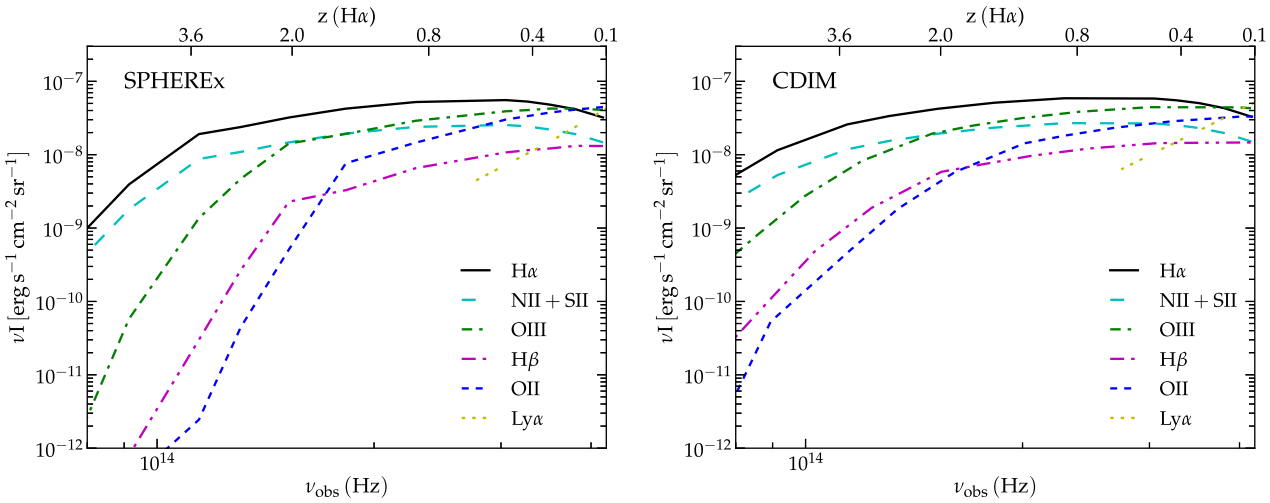

Figure 12. Intensity of several emission lines in the (0.8–4.3) × 10^{14} Hz frequency range (corresponding to a wavelength range of 3.75 − 0.70 μm), as it will be observed by the SPHEREx and CDIM surveys in galaxy survey mode. These plots were obtained from our simulation and assume both the cell resolution and the flux sensitivity of these surveys. Note that for the CDIM survey we assumed a flux sensitivity of 10^{-18} erg s^{-1} cm^{-2}. Also, for the N II and S II doublet lines we simply assumed that, following the discussion in Section 6.1, they would have 0.282 and 0.176 of the intensity of the Hα line, respectively. The intensity of Lyα emission is only shown up to $z \sim 8$, given that the intensity of this line at higher z is highly dependent on the assumed hydrogen reionization history.

7 ALTERNATIVE FOREGROUND REMOVAL/AVOIDING METHODS

In the case where the foreground removal strategies in intensity maps are not successful, CDIM and SPHEREx will still be able to use their deep surveys (in which they function as traditional galaxy surveys and resolve galaxies) for astrophysical purposes.

In Fig. 12, we show estimates for CDIM and SPHEREx constraints on bright line intensities, in order to predict how useful they will be in tracing global astrophysical quantities when operating in galaxy survey mode. Note that with the assumed flux limit for CDIM, the observed line intensity is very close to its total value. Fig. 12 indicates that at $z \sim 0 - 5$, the intensity of Hα emission should be stronger than that of the other lines. Therefore, when our target is the Hα line and the contaminant signal cannot be efficiently removed, it might be easier to estimate the Hα line intensity from the total detected intensity than through power spectrum analysis.

Fig. 12 also shows that, for $z_{\rm H\alpha} \lesssim 2$, O III line emitters are the strongest line contaminants. The ratio between the intensity of the oxygen lines relative to that of the Hα line emission is uncertain by a factor of about 2 at high redshift ($z \gtrsim 5$). The uncertainty is due to the expected decrease in galaxy metallicity with increasing redshift. This contrasts with a few of the observed high redshift galaxies, where the line ratios of oxygen lines are actually quite high. Future observations with, for example, James Webb Space Telescope (JWST) will help to further constrain these lines intensities.

Another way of separating the different line contributions is by attributing a weight to the intensity of each line and using this information together with the frequency of the emitting lines to iteratively determine the line intensities. This algorithm would take advantage of the known/fixed separation between different lines and directly fit the spectral information of all the lines intensities in a similar way to what was done for continuum infrared background data by Kogut, Dwek & Moseley (2015), although the accuracy of this method would be affected by the additional differential extinction suffered by each line.

Moreover, the possibility of using the angular information of each of the lines in an intensity map was explored by Cheng et al. (2016) for the case of C II emission line. This study uses an MCMC approach to recover the intensity and bias information from each line. For the case of Hα emission, however, this is a less promising approach, because there are several interloping lines originating from the same redshift. Moreover, the intensity of these lines is uncorrelated, whereas for C II the main contaminant lines, the different CO transitions, are highly correlated. This results in a much higher number of parameters for the case of the Hα line and so the MCMC result would be very difficult to interpret. The solution for this problem would be to independently obtain strong constraints on some of the parameters and to properly determine the correlations between them prior to using the MCMC approach.

Additionally, cross-correlating Hα intensity maps with, for example, galaxy surveys of H I radio data, as was suggested by Gong et al. (2017), can be used to avoid foreground contamination. Since, foregrounds contaminating Hα emission and H I 21 cm data are uncorrelated to first order, the cross-correlation power spectrum would make it possible to probe the signal from these two lines. The contamination by higher-order correlations in this statistical measure is unfortunately not well explored yet. Also, this procedure is limited to the cases where an H I survey covering the same position in the sky and redshift range as the Hα survey is available.

8 ASTROPHYSICAL CONSTRAINTS FROM GALAXY SURVEYS VERSUS IM SURVEYS

While galaxy surveys can observe a small fraction of the Universe in great detail, IM surveys provide a global picture of our Universe by blindly detecting emission from all types of sources. IM surveys directly probe the global quantities, whereas we can only try to infer these quantities from the limited data provided by the selection biased and flux-limited galaxy surveys.

In Fig. 13 we show the percentage of Hα emission powered by star formation that can be probed by a survey as a function of its

Downloaded from https://academic.oup.com/mnras/article-abstract/475/2/1587/4768282 by University of Groningen user on 20 March 2019

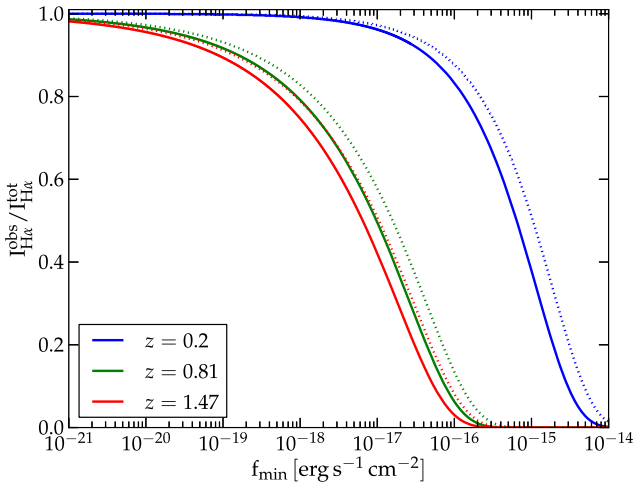

Figure 13. Fraction of H α emission powered by star formation detected by a survey as a function of its flux sensitivity. Solid and dotted lines assume, respectively, an extinction in H α emission of $A_{H\alpha} = 1$ mag and $A_{H\alpha} = 0.475$ mag. The lines shown correspond to redshifts $z = 0.2$, $z = 0.81$, and $z = 1.47$, from right to left. This figure is based on observational LFs from (Sobral et al. 2013; Stroe & Sobral 2015; Smit et al. 2016).

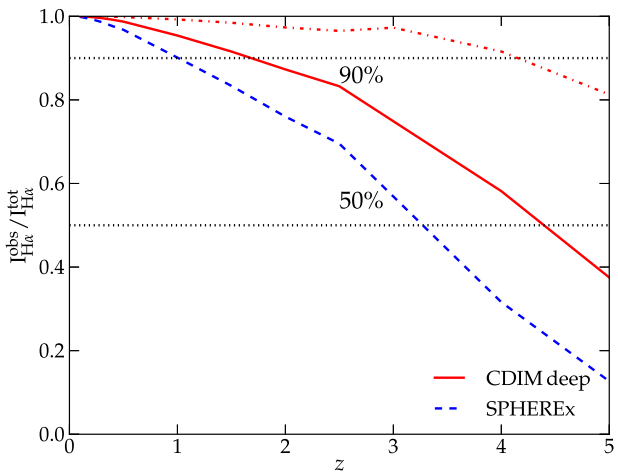

Figure 14. Intensity of H α emission powered by star formation, detected by SPHEREx (blue dashed line) and by CDIM (red lines). The red solid line assumes a flux limit of 4×10^{-18} erg s^{-1} cm^{-2}, whereas the red dashed-dotted line assumes a flux sensitivity of 1×10^{-18} erg s^{-1} cm^{-2}.

flux sensitivity. This figure is appropriate to infer the flux sensitivity limits required for a galaxy survey to be able to detect a meaningful fraction of the H α emission originating from a given redshift. In Fig. 14 we show the intensity of H α emission powered by star formation that can be detected (assuming flux sensitivity limits, at least as high as the one indicated in Table 2) by the SPHEREx and CDIM instruments. We note that using a statistical analysis, such as the power spectrum analysis, would allow the detection of emission below these flux sensitivity cuts.

Throughout this study, we mainly focus on five central points that illustrate how each of the surveys described in Table 2 is useful for astrophysical purposes and for specifically probing H α emission. These points are the survey collecting area, its flux sensitivity, the ability to distinguish between emission powered by AGN or by star formation, the certainty in the identification of the emission line responsible for the observed flux, and finally the accuracy to which the dust extinction suffered by the observed line can be determined.

We now discuss how well these points are attained for galaxy surveys, and then for IM surveys.

The properties of the *Euclid* and *WFIRST* surveys are similar, and for that reason, they will be able to detect the same types of galaxies. This study shows that, due to their sensitivity limits, these instruments will mainly detect bright galaxies. It also shows that, thanks to the planned large fields of view of these surveys, enough bright galaxies will be detected to further constrain the high luminosity end of the H α LF.

Galaxies that are bright in H α emission can vary a lot in their properties, such as in their mass or the virial mass of the DM halo they belong to. Although to a first approximation, massive galaxies are supposed to be the brightest, this will not always be true. These galaxies can suffer from quenched star formation, which would considerably decrease their H α emission. Also, massive galaxies are usually dusty galaxies and so their observed luminosity can be low. For these reasons, it is not necessarily true that the observed galaxies will correspond to a specific type of galaxy. Moreover, the observed bright galaxies might not be representative of the main H α galaxy population. As an example, bright galaxies might have particularly high- or low-luminosity ratios between different observational bands, compared to the majority of the H α emitters, which are much fainter.

Except for the small volumes magnified due to lensing, the spectroscopic surveys performed by *WFIRST* and *Euclid* will not reach the necessary low luminosities to probe the galaxies that dominate the overall H α line intensity. These surveys will also not probe the α slope (see equation 5) of the H α luminosity function, since the lensed volumes are too small to beat cosmic variance. Furthermore, the uncertainty in the modelling of the lenses itself can be considerably high, especially for highly lensed sources (Livermore, Finkelstein & Lotz 2017). These surveys might, however, help to identify the properties of a few relatively faint galaxies, given that the number density of these systems is high. Therefore, the lensed galaxies observed by *Euclid* and *WFIRST* will be important to understand the properties of low-luminosity systems and, therefore, to probe the evolution of the relation between H α emission and SFR in a galaxy.

For the *WFIRST* and *Euclid* planned surveys, the combination of the low-frequency range covered, the relatively broad photometric filters and the large number of sources that they are expected to detect, will make it impossible to properly probe the extinction suffered by each source. Line extinction will mainly be probed using galaxy templates. Although template-fitting algorithms will take into account dust extinction, it will not be possible to obtain accurate measurements for all sources, in particular for highly extinct sources (Galametz et al. 2017).

On the other hand, these galaxy surveys will be particularly good at identifying AGNs and thus in distinguishing between star formation and AGN-powered H α emission.

Moreover, *Euclid* and *WFIRST* are mainly being built with the objective of probing dark energy. For that propose, it is important to correctly identify the redshift of the source of emission. The spectroscopic and photometric capabilities of these instruments will then, at least for sources with a high signal to noise ratio (S/N >10), allow them to determine which emission line is responsible for the observed signal (Bisigello et al. 2016). Ancillary data at lower wavelengths will also be used to help identify line contaminants in these surveys (Bisigello et al. 2016).

Downloaded from https://academic.oup.com/mnras/article-abstract/475/2/1587/4768282 by University of Groningen user on 20 March 2019

The case for IM surveys is very different. The advantage of the IM surveys performed by the SPHEREx and CDIM instruments resides in their low flux limits, combined with large frequency ranges and large FOVs. These factors will allow them to probe a large fraction of the intensity of Hα emission over a large redshift range. This will also allow them to probe the time evolution of Hα emitters. Moreover, by detecting emission from the sources mainly responsible for the total intensity of the Hα line, their observational intensity maps can be used to probe the global star formation in these galaxies.

Constraining the SFRD with the SPHEREx and CDIM IM surveys will require updating the relation between Hα emission and the SFRD. These updates should be made using constraints from other emission lines obtained with the same surveys, as discussed in Section A2. Moreover, the data from IM surveys will be difficult to interpret and separate in terms of the source of the emission.

9 SUMMARY AND DISCUSSION

In this study, we explored the potential of different instruments to constrain Hα line emission. Namely, we compared the galaxy surveys that will be performed by the *Euclid* and *WFIRST* instruments, with the IM surveys that are planned for the SPHEREx and CDIM instruments.

Starting from observations, which we then extend by using physically motivated relations deduced from theory and simulations, we modelled the intensity and power spectra of the Hα line over the $z \sim 0 - 5$ redshift range.

We find that the intensity of this line is currently uncertain by a factor of up to a few until $z \sim 2$, and up to one order of magnitude at $z \sim 5$. The higher uncertainty towards high redshift lies both in the lack of observations of Hα emitters and in the increasing uncertainty of dust extinction corrections. Still, the available constraints led us to estimate that this line intensity, in the relevant redshift interval, should remain in the $I_{\mathrm{H}\alpha} \sim 10^{-8} - 10^{-7}\,\mathrm{erg\,s^{-1}\,cm^{-2}\,sr^{-1}}$ range and peak at the same time as the cosmic SFRD at $z \sim 2 - 3$.

According to the properties of the considered CDIM and SPHEREx instruments, we predict that their planned IM surveys will be good enough to make a statistical detection of the overall Hα line intensity. Moreover, when operating as a galaxy surveyor, CDIM should detect more than 90 per cent of this line intensity up to $z \sim 4 - 5$, while SPHEREx can only do the same up to $z \sim 1$. SPHEREx will still be able to detect more than 50 per cent of this emission up to $z \sim 4$. These percentages assume a minimum flux per observational voxel corresponding to the flux limits quoted for these surveys.

On the other hand, the *Euclid* and *WFIRST* galaxy surveys will only detect Hα emission in a narrow frequency range. This will include Hα emission only up to $z \sim 2$. Given their flux sensitivity limits, in spectroscopic mode, these surveys will not probe the Hα line intensity. However, they will probe the high end of the Hα LF over a large enough volume to beat cosmic variance. Moreover, at least for bright sources, *Euclid* and *WFIRST* will be able to distinguish between SF- and AGN-powered Hα emission. The photometric capabilities of these surveys will also be used to probe the galaxy dust extinction and to help distinguish between emission from different lines. These two points will only be easily achievable for relatively bright galaxies.

Using the same methodology as for the Hα line, we modelled the emission by the S II and N II doublet lines and by the O II, O III, Hβ, and Lyα lines in the redshift range where these lines will contaminate Hα intensity maps. We found that for a survey not suffering from flux limitations, the signal from contaminant lines will increase the observed Hα power spectra by a factor up to 2 at $z \lesssim 2$. At higher redshift this contamination is expected to decrease.

We implemented the several models for line emission in a simulation code and obtained a light cone for both the Hα line and the background contaminant lines. The observational light cones assume the flux sensitivity and voxel resolution of each of the planned IM surveys. We find that, besides the contamination by background interloping lines being quite strong (in terms of both intensity and power spectrum), it is also difficult to remove.

We applied flux cuts to the background lines of (3.0, 1.2, 0.5) $\times\ 10^{-16}\,\mathrm{ergs\,s^{-1}\,cm^{-2}}$, in order to estimate the effect that a masking procedure would have on the contamination power spectrum. We find that the required flux cuts for masking need to be stronger towards increasing redshift. Still, overall they were successful at decreasing the contamination power spectrum to a maximum of $\sim$10 per cent of the observed Hα signal. The removal of contamination by these bright background galaxies would only require masking less than 1 per cent of the voxels for both the SPHEREx and the CDIM surveys. The decrease in the Hα power spectrum due to putting the strongly contaminated voxels to zero would also be below 1 per cent. The recovery of the target signal would thus not be compromised.

At $z \lesssim 0.8$, the detection of interloping contaminants in Hα intensity maps can be reasonably done with data from a galaxy survey with a flux sensitivity of $1.2 \times 10^{-16}\,\mathrm{ergs\,s^{-1}\,cm^{-2}}$. This corresponds to the sensitivity of the *WFIRST* instrument, although it lies outside the frequency range covered by this survey. For Hα intensity maps in the range $z \sim 0.8$–2, a flux cut of $5.0 \times 10^{-17}\,\mathrm{ergs\,s^{-1}\,cm^{-2}}$ would produce a similar reduction of the contaminants power spectrum. Unfortunately, there is no available galaxy survey that can detect contaminant galaxies up to this low flux level and over the large volumes covered by the IM surveys.

Given the lack of surveys that can individually detect the main contaminant galaxies, we believe that the best option for Hα IM studies is to jointly model the evolution of all the strong emission lines contributing to the observed line fluxes. After recovering the observed Hα signal, intensity maps should be corrected for dust extinction. We explored the possibility of doing this with the data from the same IM surveys and found that this can be done, to a certain point, using ratios of emission lines. This would require efficient separation of the contribution from the different lines in these intensity maps, which is not trivial. Alternatively, the extinction rates and extinction curves from galaxy surveys can be used to at least predict the overall evolution of the dust extinction rate at the relevant frequencies.

We, therefore, conclude that IM surveys can be used to probe the overall intrinsic Hα intensity up to an uncertainty of the order of 20 per cent, as long as this line signal can be accurately disentangled from the signal of other emission lines.

Many of our results are biased towards our choice of using a high redshift SFRD model based on observations of Hα emitters. These have inferred SFRs higher than the SFRs traced by the UV continuum. Despite the reasons for this discrepancy, our choice allowed us to make predictions for the Hα intensity and power spectrum consistent with observations. Moreover, O III emitters, which are the most important contaminants in Hα intensity maps, also have very large EWs at high z. Consequently, our SFRD-based predictions for the intensity of this line are consistent with observational constraints. In the case of O III emitters the large EWs are likely to be the

Downloaded from https://academic.oup.com/mnras/article-abstract/475/2/1587/4768282 by University of Groningen user on 20 March 2019

result of the high ionized state of the ISM in high redshift galaxies. Therefore, we might be overestimating the contamination by H β and O II emitters. However, this does not affect our main conclusions, given the small contribution from these lines ($\lesssim$10 per cent) to the contamination power spectra in H α intensity maps.

ACKNOWLEDGEMENTS

The authors thank the anonymous referee whose comments and suggestions helped to improve the quality of the article. We also thank the Netherlands Foundation for Scientific Research support through the VICI grant 639.043.006.

REFERENCES

Alonso D., Bull P., Ferreira P. G., Santos M. G., 2015, MNRAS, 447, 400
Amendola L. et al., 2013, Living Rev. Relat., 16, 6
Anders P., Fritze-v. Alvensleben U., 2003, A&A, 401, 1063
Behroozi P. S., Wechsler R. H., Conroy C., 2013, ApJ, 770, 57
Bisigello L. et al., 2016, ApJS, 227, 19
Boutsia K. et al., 2011, ApJ, 736, 41
Boylan-Kolchin M., Springel V., White S. D. M., Jenkins A., Lemson G., 2009, MNRAS, 398, 1150
Bruzual A. G., Charlot S., 1993, ApJ, 405, 538
Calzetti D., Armus L., Bohlin R. C., Kinney A. L., Koornneef J., Storchi-Bergmann T., 2000, ApJ, 533, 682
Cantalupo S., Porciani C., Lilly S. J., 2008, ApJ, 672, 48
Capak P. et al., 2007, ApJS, 172, 99
Castellano M. et al., 2017, ApJ, 839, 73
Chabrier G., 2003, PASP, 115, 763
Chang T.-C., Pen U.-L., Bandura K., Peterson J. B., 2010, Nature, 466, 463
Cheng Y.-T., Chang T.-C., Bock J., Bradford C. M., Cooray A., 2016, ApJ, 832, 165
Coil A. L. et al., 2015, ApJ, 801, 35
Colbert J. W. et al., 2013, ApJ, 779, 34
Cole S., Lacey C. G., Baugh C. M., Frenk C. S., 2000, MNRAS, 319, 168
Cole S. et al., 2001, MNRAS, 326, 255
Comaschi P., Ferrara A., 2016, MNRAS, 455, 725
Cooray A. et al., 2016, preprint (arXiv:1602.05178)
Dopita M. A., Kewley L. J., Sutherland R. S., Nicholls D. C., 2016, Ap&SS, 361, 61
Doré O. et al., 2014, preprint (arXiv:1412.4872)
Doré O. et al., 2016, preprint (arXiv:1606.07039)
Drake A. B. et al., 2013, MNRAS, 433, 796
Fonseca J., Silva M. B., Santos M. G., Cooray A., 2017, MNRAS, 464, 1948
Galametz A., Saglia R., Paltani S., Apostolakos N., Dubath P., 2017, A&A, 598, A20
Gallego J., Zamorano J., Aragon-Salamanca A., Rego M., 1995, ApJ, 455, L1
Garn T., Best P. N., 2010, MNRAS, 409, 421
Geach J. E., Smail I., Best P. N., Kurk J., Casali M., Ivison R. J., Coppin K., 2008, MNRAS, 388, 1473
Geach J. E., Sobral D., Hickox R. C., Wake D. A., Smail I., Best P. N., Baugh C. M., Stott J. P., 2012, MNRAS, 426, 679
Gehrels N., Spergel D., WFIRST SDT Project, 2015, J. Phys. Conf. Ser., 610, 012007
Gill S. P. D., Knebe A., Gibson B. K., 2004, MNRAS, 351, 399
Gong Y., Cooray A., Silva M., Santos M. G., Bock J., Bradford C. M., Zemcov M., 2012, ApJ, 745, 49
Gong Y., Silva M., Cooray A., Santos M. G., 2014, ApJ, 785, 72
Gong Y., Cooray A., Silva M. B., Zemcov M., Feng C., Santos M. G., Dore O., Chen X., 2017, ApJ, 835, 273
Gordon K. D., Clayton G. C., Misselt K. A., Landolt A. U., Wolff M. J., 2003, ApJ, 594, 279
Green J. et al., 2012, preprint (arXiv:1208.4012)
Guo Q., White S., Angulo R. E., Henriques B., Lemson G., Boylan-Kolchin M., Thomas P., Short C., 2013, MNRAS, 428, 1351
Haardt F., Salvaterra R., 2015, A&A, 575, L16
Hayashi M., Sobral D., Best P. N., Smail I., Kodama T., 2013, MNRAS, 430, 1042
Hopkins A. M., Beacom J. F., 2006, ApJ, 651, 142
Hopkins A. M., Connolly A. J., Szalay A. S., 2000, AJ, 120, 2843
Hunt L., Dayal P., Magrini L., Ferrara A., 2016, MNRAS, 463, 2002
Kennicutt R. C., Jr, 1998a, ARA&A, 36, 189
Kennicutt R. C., Jr, 1998b, ApJ, 498, 541
Kewley L. J., Groves B., Kauffmann G., Heckman T., 2006, MNRAS, 372, 961
Kewley L. J., Dopita M. A., Leitherer C., Davé R., Yuan T., Allen M., Groves B., Sutherland R., 2013a, ApJ, 774, 100
Kewley L. J., Maier C., Yabe K., Ohta K., Akiyama M., Dopita M. A., Yuan T., 2013b, ApJ, 774, L10
Khostovan A. A., Sobral D., Mobasher B., Best P. N., Smail I., Stott J. P., Hemmati S., Nayyeri H., 2015, MNRAS, 452, 3948
Khostovan A. A., Sobral D., Mobasher B., Smail I., Darvish B., Nayyeri H., Hemmati S., Stott J. P., 2016, MNRAS, 463, 2363
Kobulnicky H. A., Kewley L. J., 2004, ApJ, 617, 240
Kogut A., Dwek E., Moseley S. H., 2015, ApJ, 806, 234
Kooistra R., Silva M. B., Zaroubi S., 2017, MNRAS, 468, 857
Kroupa P., Weidner C., 2003, ApJ, 598, 1076
Laureijs R. et al., 2011, preprint (arXiv:1110.3193)
Lee J. C. et al., 2009, ApJ, 706, 599
Lewis A., Challinor A., Lasenby A., 2000, ApJ, 538, 473
Lidz A., Furlanetto S. R., Oh S. P., Aguirre J., Chang T.-C., Doré O., Pritchard J. R., 2011, ApJ, 741, 70
Livermore R. C., Finkelstein S. L., Lotz J. M., 2017, ApJ, 835, 113
Ly C. et al., 2007, ApJ, 657, 738
Madau P., Dickinson M., 2014, ARA&A, 52, 415 (MD+14)
Madau P., Ferguson H. C., Dickinson M. E., Giavalisco M., Steidel C. C., Fruchter A., 1996, MNRAS, 283, 1388
Madau P., Meiksin A., Rees M. J., 1997, ApJ, 475, 429
Mármol-Queraltó E., McLure R. J., Cullen F., Dunlop J. S., Fontana A., McLeod D. J., 2016, MNRAS, 460, 3587
Masui K. W. et al., 2013, ApJ, 763, L20
Matthee J., Sobral D., Darvish B., Santos S., Mobasher B., Paulino-Afonso A., Röttgering H., Alegre L., 2017, MNRAS, 472, 772
McQuinn K. B. W., Skillman E. D., Dolphin A. E., Mitchell N. P., 2015, ApJ, 808, 109
Mitchell P. D., Lacey C. G., Baugh C. M., Cole S., 2016, MNRAS, 456, 1459
Osterbrock D. E., 1989, Astrophysics of Gaseous Nebulae and Active Galactic Nuclei. University Science Books, Mill Valley, CA
Osterbrock D. E., Ferland G. J., 2006, Astrophysics of Gaseous Nebulae and Active Galactic Nuclei. University Science Books, Sausalito, CA
Peters T. et al., 2017, MNRAS, 466, 3293
Planck Collaboration XVI, 2014, A&A, 571, A16
Popping G., Somerville R. S., Galametz M., 2017, MNRAS, 471, 3152
Pozzetti L. et al., 2016, A&A, 590, A3
Pritchard J. R., Loeb A., 2012, Rep. Progr. Phys., 75, 086901
Pullen A. R., Doré O., Bock J., 2014, ApJ, 786, 111
Raga A. C., Castellanos-Ramírez A., Esquivel A., Rodríguez-González A., Velázquez P. F., 2015, RMxAA, 51, 231 (Raga+15)
Salpeter E. E., 1955, ApJ, 121, 161
Santos S., Sobral D., Matthee J., 2016, MNRAS, 463, 1678
Saunders W., Rowan-Robinson M., Lawrence A., Efstathiou G., Kaiser N., Ellis R. S., Frenk C. S., 1990, MNRAS, 242, 318
Schechter P., 1976, ApJ, 203, 297
Schlegel D. J., Finkbeiner D. P., Davis M., 1998, ApJ, 500, 525
Scoville N., Faisst A., Capak P., Kakazu Y., Li G., Steinhardt C., 2015, ApJ, 800, 108
Shim H., Colbert J., Teplitz H., Henry A., Malkan M., McCarthy P., Yan L., 2009, ApJ, 696, 785
Silva M. B., Santos M. G., Gong Y., Cooray A., Bock J., 2013, ApJ, 763, 132

Downloaded from https://academic.oup.com/mnras/article-abstract/475/2/1587/4768282 by University of Groningen user on 20 March 2019

Silva M., Santos M. G., Cooray A., Gong Y., 2015, ApJ, 806, 209
Silva M. B., Kooistra R., Zaroubi S., 2016, MNRAS, 462, 1961
Smit R., Bouwens R. J., Labbé I., Franx M., Wilkins S. M., Oesch P. A., 2016, ApJ, 833, 254
Sobral D. et al., 2009, MNRAS, 398, 75
Sobral D., Best P. N., Matsuda Y., Smail I., Geach J. E., Cirasuolo M., 2012, MNRAS, 420, 1926
Sobral D., Smail I., Best P. N., Geach J. E., Matsuda Y., Stott J. P., Cirasuolo M., Kurk J., 2013, MNRAS, 428, 1128
Sobral D. et al., 2015, MNRAS, 451, 2303
Sobral D., Kohn S. A., Best P. N., Smail I., Harrison C. M., Stott J., Calhau J., Matthee J., 2016a, MNRAS, 457, 1739
Sobral D., Stroe A., Koyama Y., Darvish B., Calhau J., Afonso A., Kodama T., Nakata F., 2016b, MNRAS, 458, 3443
Sparre M. et al., 2015, MNRAS, 447, 3548
Spergel D. et al., 2015, preprint (arXiv:1503.03757)
Springel V., 2005, MNRAS, 364, 1105
Springel V., Yoshida N., White S. M., 2001, New Astron, 6, 79
Springel V. et al., 2005, Nature, 435, 629
Stroe A., Sobral D., 2015, MNRAS, 453, 242
Suzuki T. L. et al., 2016, MNRAS, 462, 181
Thacker C. et al., 2013, ApJ, 768, 58
Uzgil B. D., Aguirre J. E., Bradford C. M., Lidz A., 2014, ApJ, 793, 116
Vasei K. et al., 2016, ApJ, 831, 9
Villar V., Gallego J., Pérez-González P. G., Barro G., Zamorano J., Noeske K., Koo D. C., 2011, ApJ, 740, 47
Visbal E., Loeb A., 2010, JCAP, 1011, 016
Yajima H., Li Y., Zhu Q., Abel T., Gronwall C., Ciardullo R., 2014, MNRAS, 440, 776
Yan L., McCarthy P. J., Freudling W., Teplitz H. I., Malumuth E. M., Weymann R. J., Malkan M. A., 1999, ApJ, 519, L47

APPENDIX A: CONSTRAINTS FROM IM AND GALAXY SURVEYS

A1 Constraints on the properties of H α line emitters

In this appendix, we discuss, in some detail, different constraints on galaxy properties that can be achieved by galaxy and IM surveys targeting H α emission.

In order to properly constrain H α emission, a survey needs to cover a large volume to overcome cosmic variance. It also has to be sensitive enough to detect emission from relatively faint sources in order to probe a large fraction of the overall intensity of line emission. Moreover, it should cover a large bandwidth in frequency to probe the target signal over a large redshift/time range and to allow for the identification and removal of line contaminants. Spatial and spectral resolution is also important if one wishes to identify the individual sources of emission, or at least to differentiate between star-forming systems and active galactic nuclei. Furthermore, the ability to determine the extinction suffered by the H α line is needed to probe this line intrinsic luminosity.

We now describe, in some detail, how each of the surveys described in Section 5 can satisfy the above-listed requirements to constrain H α emission.

A1.1 Cosmic variance

Euclid and *WFIRST* aim to detect and characterize H α emission from high-luminosity galaxies. Massive, luminous galaxies are preferentially located in the high-density peaks and so these instruments are required to survey a large fraction of the sky in order to beat cosmic variance. This implies covering volumes of the order of 5×10^5 Mpc^3, just to beat cosmic variance in H α emission at the 90 per cent level (Sobral et al. 2015).

The combination of *Euclid*'s deep survey frequency resolution and its field of view (FOV) translates to a volume per redshift bin too small to beat cosmic variance. As a result, *Euclid*'s data of bright galaxies will have to be averaged in three or four frequency bins before being used for H α studies. This will not be necessary for *WFIRST* data due to its impressive 2227 deg^2 FOV. Both the SPHEREx deep survey and CDIM wide survey will cover large enough volumes to beat cosmic variance.

A1.2 Sensitivity

The observed characteristic H α luminosity, $L^{\star}_{\rm H\alpha}$, scales as $\log L^{\star}_{\rm H\alpha}[{\rm erg\,s^{-1}}] = 0.45z + 41.47$ over the redshift range $z = 0 - 2.23$ (Sobral et al. 2016a).

The *Euclid* and *WFIRST* spectroscopic surveys will be able to constrain the H α LF above the characteristic luminosity at $z \sim 0.7$ and $z \sim 1.1$, respectively. However, since galaxies below the $L^{\star}_{\rm H\alpha}$ luminosity still contribute significantly to this line LF, these instruments will not have enough sensitivity to constrain the overall H α intensity. Note that their photometric surveys will be much better at constraining this intensity.

In the case of IM surveys performed by the CDIM and the SPHEREx instruments, the lines intensities can be totally recovered using statistical methods. Moreover, the signal in bright voxels of the observed maps can be independently detected as is done with traditional galaxy survey data. In that case, only the voxels with a signal above the noise can be recovered, where the noise in the map is given by the flux sensitivity of the IM survey listed in Table 2.

The surveys planned for CDIM and SPHEREx will have better flux sensitivities than those performed by *Euclid* or *WFIRST*. Therefore, these IM surveys should be able to directly probe the H α intensity in most voxels at low z and a reasonable fraction of this signal at higher z. CDIM can do much better than SPHEREx on this point, as is shown in Fig. 14. This figure shows that in CDIM intensity maps, the H α signal should be above the noise level in close to 80 per cent of the voxels at $z \sim 5$. Moreover, this percentage will increase towards lower redshifts.

A1.3 Contamination

AGN contamination: AGNs mostly populate the high end of the H α LF. The number density of AGN, contributing to the H α LF, at $z < 2.3$ is fairly constant (Sobral et al. 2016a). Given the expected evolution of star-forming H α emitters, the AGN fractional contribution to the overall H α intensity is expected to increase from $z = 0$ towards the peak of star formation activity. However, the H α line intensity will remain dominated by fainter star-forming galaxies (Sobral et al. 2016a). Moreover, the bright AGN population should rapidly decline at $z \simeq 3$, which will consequently decrease its contribution to the H α intensity (Haardt & Salvaterra 2015).

By integrating over the H α luminosity function and assuming that the AGN population corresponds to 30 per cent of the observed H α emitters (see Sobral et al. 2016a), the derived number density of bright AGN is of the order of 10^{-4} Mpc^{-3}.

For very bright sources, *Euclid* and *WFIRST* surveys will be sensitive enough to differentiate between H α emission powered by AGN activity or by star formation. In these surveys, AGN will be identified as sources with Balmer lines with FWHM above 1000 km s^{-1}. When possible, AGN will also be identified using emission line flux ratios (see Sobral et al. 2016a).

In IM surveys data, the sources of H α photons are completely blended together. Nevertheless, thanks to the increasing number of

Downloaded from https://academic.oup.com/mnras/article-abstract/475/2/1587/4768282 by University of Groningen user on 20 March 2019

AGN detected at high-z, the brightest AGN can be masked from intensity maps significantly reducing their signal.

The voxels from the SPHEREx surveys have volumes of the order of a few Mpc^3 whereas the voxels from CDIM surveys are even smaller. Therefore, contamination by bright AGN should be present in a small percentage of the voxels of the observed intensity maps.

There will not be enough information about AGN at high redshifts to mask all these galaxies from intensity maps. However, their overall contribution to the H α intensity, as predicted by integrating over current H α LFs, should be below the 1 per cent level.

The identification of AGN in the presence of multiwavelength data is further discussed in Section B1.

Line contamination: H α observations will suffer strong contamination from several background lines. Surveys covering a large frequency range with a relatively high spectral resolution are necessary to allow for an accurate identification of the emission line responsible for the observed signal.

Euclid and *WFIRST* will obtain low-resolution spectra of the energy distribution of resolved galaxies emission. This will, in some cases, allow for the identification of the targeted emission line. At this point, *Euclid* will have the advantage over *WFIRST*, given its higher spectral resolution.

IM surveys do not resolve emission sources. For these surveys, additional, independent surveys are used to identify bright interloping lines. Alternatively, the signal of several emission lines can be fitted to power spectra derived from the intensity maps at different redshifts. This can potentially be used to separate the emission in different emission lines.

A1.4 Dust extinction

Both galaxy surveys and IM surveys will be sensitive to the H α radiation that escaped the galaxy without being absorbed by the dust in the ISM. However, for astrophysical studies, the relevant quantity is the intrinsic H α emission and so the observed H α emission has to be corrected for dust extinction.

Dust extinction is usually measured by fitting a galaxy emission spectra and/or with observed ratios of emission lines. Most commonly, H α line extinction in the ISM is estimated from the observed fluxes in the Balmer H α and H β emission lines. The emission rates of recombination and collisional excitation of these lines scale approximately in the same way with the gas temperature and ionization state. Therefore, the intrinsic ratio between these lines fluxes is expected to follow the ratio $f^i_{\mathrm{H}_\beta}/f^i_{\mathrm{H}_\alpha} = 0.35$, as mentioned in Section 6.1. With this method, the magnitude of extinction suffered by the H α line is:

$$A_{\mathrm{H}\alpha} = \frac{-2.5\,k_{\mathrm{H}\alpha}}{k_{\mathrm{H}\beta} - k_{\mathrm{H}\alpha}} \log_{10} \frac{f^i_{\mathrm{H}\alpha}/f^i_{\mathrm{H}\beta}}{f_{\mathrm{H}\alpha}/f_{\mathrm{H}\beta}}, \tag{A1}$$

where $f_{\mathrm{H}\alpha}$ and $f_{\mathrm{H}\beta}$ refer, respectively, to the observed line fluxes in the H α and H_β lines and the index i denotes the intrinsic line fluxes (Sobral et al. 2012). We assume the dust absorption coefficients, $k_{\mathrm{H}\alpha}$ and k_β, given by the Calzetti et al. (2000) extinction curve. The H α dust extinction is therefore

$$A_{\mathrm{H}\alpha} = 6.531 \log_{10} f_{\mathrm{H}\alpha}/f_{\mathrm{H}\beta} - 2.981. \tag{A2}$$

This equation will be used to estimate the dust extinction suffered by bright galaxies in the galaxy surveys data. *Euclid* will detect both the H α and H β fluxes, for H α emitters in the redshift range $z \sim 1.29 - 2.04$. While *WFIRST* will only be able to do the same in the much smaller $z \sim 1.8$–1.96 redshift range. *Euclid* and *WFIRST* spectroscopic surveys will cover frequency ranges to narrow to allow us to properly fit a galaxy spectra. Therefore, when no other constraints are available, these missions will rely on dust extinction rates estimated from the relative intensities in their B and V filters (Galametz et al. 2017).

The relatively large frequency range covered by IM surveys allows for the use of several different methods to probe the overall H α dust extinction. For these surveys, dust extinction will be estimated using flux ratios of high transition hydrogen lines, flux ratios of metal lines, by fitting low-resolution spectra, and by taking advantage of extinction rates derived from other missions.

At the local Universe, SPHEREx will map the entire sky, with Paschen-α (1875 nm) and Brackett-α (4051 nm) recombination lines. These lines are intrinsically weaker than the H α line, but they suffer less dust extinction than the Balmer H α and H β lines and so they are better probes of galaxy properties. At $z \lesssim 0.5$, the amount of dust extinction will be probed using features in low-resolution spectra of millions of galaxies per bin. At $z \sim 1$, this survey will make use of photometry from LSST and other surveys in order to probe the dust content of the galaxies. Finally, at $z \sim 1.36$, SPHEREx will be able to use the H β plus the O III [500.7 nm] lines to estimate the dust extinction in the galaxy. These data will also be compared to galaxy SEDs derived from previous surveys in the same redshift ranges, as described in Doré et al. (2016)

In order to probe for dust extinction, the proposed CDIM mission will have all the resources available for SPHEREx. Additionally, CDIM will have a higher frequency resolution which allows for the separation between emission in very close lines. This is essential for the SED fitting technique to be successful. Therefore, CDIM will provide more reliable estimates of H α dust extinction than SPHEREx.

Since there is no observational basis indicating that dust extinction curves evolve considerably up to $z \sim 5$, the main source of uncertainty in the extinction magnitudes derived from observed line flux ratios, involving metal lines, are the assumed intrinsic flux ratios.

The intrinsic fluxes, of hydrogen lines, scale mainly with the intensity of the ionizing radiation, which is one of the galaxy properties more easily accessible to observations. On the other hand, the fluxes of metal lines also depend strongly on additional galaxy properties, such as gas clumping, metallicity, and hardness of the ionizing spectrum. The redshift evolution of these additional galaxy properties is not easy to infer from observations, as discussed in Section A2.

At redshift windows where an estimation of the dust extinction cannot be made, the intrinsic H α emission cannot be recovered up to a 20–40 per cent correction factor.

A2 Constraints on ISM gas metallicity and ionization state

The Universe at high redshifts was considerably younger and so galaxy properties such as IMF, metallicity, and SED might have been very different from today's galaxies.

High-z observations are often interpreted using relations based on observations at very low-z. The evolution of galaxy properties will thus affect the reliability of the interpretation of high-z observational data. This problem can be mitigated using multiwavelength sets of data to confirm/constrain key properties of high-z galaxies.

Current constraints indicate that, although galaxy metallicity is a function of stellar mass and SFR, this dependence shows little to no evolution up to $z \sim 3.7$ (Hunt et al. 2016). At higher z, there are no available observations that can confirm or refute this trend.

Downloaded from https://academic.oup.com/mnras/article-abstract/475/2/1587/4768282 by University of Groningen user on 20 March 2019

Towards very high-z ($z \gtrsim 6$), however, galaxies are expected to be more metal-poor, due to the low amount of time available for the stars to pollute the ISM with metals, and so the intrinsic ratios of metal line fluxes to the galaxy SFR should decrease.

The dust-to-gas mass ratio in the ISM scales with metallicity since a substantial fraction of heavy elements is part of the dust composition. Simulations predict that the average dust mass density in the ISM declines by around 1 order of magnitude from $z \sim 0$ to $z \sim 5$ (Popping, Somerville & Galametz 2017). On the observational side, infrared emission by dust seems to be consistent with no evolution in the ISM dust mass up to a redshift of $z \sim 2.3$ (Thacker et al. 2013). In the near future, observations of individual galaxies by the ALMA and JWST instruments should confirm or refute these trends.

Galaxy surveys can probe the metallicity of galaxies through their emission spectra or with ratios of strong metal lines, namely carbon, oxygen, and nitrogen lines. The *Euclid* and *WFIRST* surveys will provide low-resolution spectra that can only be used to constrain the properties of very bright galaxies. They will also probe galaxy metallicity and ionization state using the EW of the O III emission line, which will be detected in the redshift range [1.2/1.7, 3.0] for, respectively, the *Euclid* and *WFIRST* surveys. These surveys will span a narrow frequency range which will not allow them to detect many metal lines in overlapping redshift ranges. Therefore, the *Euclid* and *WFIRST* missions plan to make use of data from other instruments/surveys to probe more frequency bands and so to further constrain their galaxy spectra.

In the case of IM surveys, the relative intensity of emission lines can be used for this same objective. Due to their large frequency range, the described IM surveys will be able to detect the integrated emission from the Hα, Hβ, O II, and O III lines at $z \sim 0.87 - 5$.

In intensity maps, the signal from different lines will be blended together. However, there are frequency windows where a specific line dominates the total intensity in an observational voxel (Fonseca et al. 2017). This can be used to help disentangle the contribution from each line so that their intensities can at least be fitted as a function of redshift. In that case, these line intensities can be used to constrain the overall galaxy metallicity and ionization parameter. A method to do this is described in detail in Section B2.

A3 Constraints on the SFRD

Prior to being used in SFR studies, the observed Hα signal needs to be corrected for line contamination, AGN emission, and dust extinction as discussed, respectively, in Section 6 and in Section A1. Moreover, in order to constrain the SFRD the Hα luminosity density needs to be probed, which implies observing down to relatively faint levels.

As is clear from Fig. 13, the spectroscopic surveys performed by *Euclid* and *WFIRST* will not have enough sensitivity to probe the overall Hα luminosity density. As a result, on their own, these surveys will not be able to constrain the cosmic SFRD. They will, however, be able to individually detect and identify many AGNs. *Euclid* and *WFIRST* will use their photometric surveys to detect fainter Hα emitters, but not faint enough to constrain the overall Hα emission. These instruments photometry will also be helpful in estimating the dust extinction suffered by the Hα line.

IM surveys should be able to make a statistical detection of the full Hα signal. The observed signal will be contaminated by several interloping lines. However, either by masking the contaminated voxels or by fitting the emission from the several lines, the Hα intensity as a function of redshift should be recovered with reasonable accuracy, as discussed in Section 6. The dust extinction suffered by this line can also be estimated using the procedures described in Section A1.4. Moreover, the contribution from AGN, to the total Hα intensity, is relatively small and in principle the brightest AGN can be masked in the observational maps, as discussed in Section A1.3.

IM surveys will, therefore, be able to constrain the intrinsic Hα intensity reasonably well up to $z \sim 5$.

The SFR can be inferred from the intrinsic Hα luminosity using equation (3). The physics connecting Hα emission and SFR sets the coefficient in this equation. At low redshift, there are enough observations to constrain this coefficient, however, that is not the case at high-z ($z \gtrsim 2$). The validity and accuracy of this coefficient depend on the following assumptions:

(i) The gas is in ionization equilibrium at a temperature of $T = 10^4$ K and Hα photons are mainly emitted during recombinations. Detailed simulations of the ISM and comparison with observations indicate that, at solar metallicity, collisional excitations contribute to about ~1–10 per cent of the total Hα emission (Peters et al. 2017). Higher contributions would require very strong UV fields that would destroy molecular clouds and cause a subsequent decline in the galaxy star formation rate. There are not many observational constraints at high redshift and so collisional excitations cannot be safely ignored if we allow the gas to be at a higher temperature, as is shown in Fig. 6.

(ii) All UV ionizing photons are spent on ionizing the ISM gas. This gas will eventually recombine, emitting several line photons. This premise assumes that the escape fraction of ionizing UV radiation is very close to zero, which is consistent with the small number of observational constraints at low redshift. On the other hand, a larger escape fraction is expected towards higher redshifts in order to account for the intensity of the UVB radiation and to explain the reionization of hydrogen gas.

(iii) The probability of emission of an Hα photon per hydrogen recombination is $f_{\rm rec} = 0.45$. In reality, this factor will depend on the galaxy IMF and on the strength of the UV field. At the local Universe, the assumed $f_{\rm rec}$ value is consistent with observations, but towards high redshifts, there is a discrepancy between SFRDs derived from Hα fluxes and from continuum UV luminosities (Smit et al. 2016). This discrepancy might be explained with bursty star formation episodes, boosting the Hα emission (hypothesis discouraged by observations). It can also be explained by a particularly strong UV radiation, which would be a consequence of changes in the IMF and/or in the UV β slope (supported by observations). An alternative explanation would be that the dust extinction curve assumed is wrong and consequently the relation between the extinction in the two frequency bands would be different from what is assumed. The future JWST will help to identify the source of this discrepancy and confirm if there is any meaningful redshift evolution in the amount of dust or in the galaxy spectral energy distribution.

Despite the several issues pointed out above, the coefficient between Hα emission and the SFR can be adjusted using future observational data. As a result Hα luminosity density can be used as a good tracer of the global SFRD even at high redshifts.

A4 Constraints on the stellar mass

The most reliable way to estimate a galaxy stellar mass is likely to be fitting the galaxy emission spectra to theoretical templates of galaxies SED. However, this method will work only when the

Downloaded from https://academic.oup.com/mnras/article-abstract/475/2/1587/4768282 by University of Groningen user on 20 March 2019

galaxy SEDs is well constrained and even then its accuracy depends on the validity of the templates used.

There are multiple galaxy properties that have a similar impact on a galaxy SED. For example, the age of a galaxy, metallicity, and dust extinction will all affect the same frequency range corresponding to the red band. Note that towards high redshifts, galaxies will be all relatively younger (due to the young age of the Universe) and dust extinction and metallicity will be smaller, making the stellar mass estimates more robust.

Alternatively, the stellar mass of a galaxy can be inferred from ratios of fluxes in two frequency band or from the intensity of some emission lines. This method has the advantage that the degeneracy between many of the parameters that shape a galaxy SED can be broken or minimized by using ratios between emission lines.

The connection between galaxies stellar mass and ratios between fluxes in different bands or the strength of an emission line is biased towards the chosen IMF. By default, in studies of the high redshift Universe, it is assumed that galaxies follow a Salpeter IMF. A heavier IMF would result in a smaller stellar mass as inferred from line emission data. Moreover, a galaxy SED affects extinction curve of a galaxy. Prescriptions to improve upon extinction estimates suffered by an emission lines, when the galaxy SED is unknown, are discussed in Galametz et al. (2017).

For *Euclid* and *WFIRST*, bright galaxies stellar mass will be estimated by fitting the observed low-resolution spectra to theoretical templates. The wavelength range covered by *Euclid* and *WFIRST* corresponds to the *R* band, where extinction is not as high as in the *UV* band. It is still an important issue, however. The photometric capabilities of these missions will allow for the estimation of the galaxy metallicity through the diagnostic R_{23} ratio given by:

$$\log R_{23} \equiv \left(\frac{I_{[\mathrm{O\,II}]\lambda 3727} + I_{[\mathrm{O\,III}]\lambda 4959} + I_{[\mathrm{O\,III}]\lambda 5007}}{I_{\mathrm{H}\beta}} \right). \tag{A3}$$

These estimates will be somewhat unreliable, given that the frequency band covered by each filter is very large. Therefore, a filter will collect emission from several transition lines. Also, the redshift range for which the estimate of the R_{23} ratio is possible is small.

IM surveys will not be able to measure galaxies spectra. However, the SPHEREx and CDIM surveys will reach near-infrared wavelengths, where dust extinction is relatively small, and so these instrument surveys can potentially provide good estimates of galaxy stellar mass.

At low redshift, SPHEREx will map galaxy emission in the Paschen and Bracket hydrogen recombination lines. These are infrared lines and so they suffer from very low extinction, which makes them relatively good probes of galaxy stellar mass and star formation rate. The sensitivity of SPHEREx will only allow it to probe these emission lines in bright galaxies, down to a stellar mass of $\sim 10^{10}\,\mathrm{M}_{\odot}$. This lower limit on the stellar mass is high compared to the stellar mass range that is currently probed by other instruments targeting H α emission (Villar et al. 2011; Sobral et al. 2016b). On the other hand, CDIM has a higher sensitivity than SPHEREx, by about one order of magnitude, and so it should be able to detect galaxies with stellar masses as low as the current high-*z* galaxy surveys.

In simulations such as Illustris, a tight correlation between star formation and stellar mass has been found at a fixed redshift (Sparre et al. 2015). Under this assumption, stellar mass can be estimated from the SFR derived from line emission observations. However, given the lack of observational constraints on the high-*z* ratio between star formation and stellar mass, it is advisable to use several line probes to confirm this relation. This is possible since some line strengths scale with the galaxy instantaneous SFR (such as the H α line), whereas others are proportional to the galaxy gas content or its stellar mass.

APPENDIX B: MULTIWAVELENGTH DATA

In the presence of multiwavelength data, the constraints from high-*z* observations will become a lot more reliable. Therefore, all the missions discussed in this study will try to use all their available data to improve/confirm their conclusions. In this section we present some strategies involving multiwavelength data relevant for these missions. Moreover, we discuss some of the limitations associated with these methods.

B1 Identifying AGN

The Baldwin–Phillips–Terlevich (BPT) diagram can be used to distinguish AGN from purely star-forming galaxies using the O III/H β and N II/H α line ratios. This diagram has been updated by Kewley et al. (2013b), in order to be compatible with the redshift evolution of the ISM of star-forming galaxies. There are, however, selection biases associated with the BPT diagram that cause some AGN in low mass and/or in high specific star formation rate galaxies to be missed (Coil et al. 2015). This is increasingly problematic towards high redshift.

B2 Constraining galaxies ISM

In the presence of fluxes from the H α, H β, O II, and O III lines, many ISM properties can be determined by iteratively converging the following set of equations, taken from Kobulnicky & Kewley (2004).

The relative intensity on many lines depends on the ionization state of the emitting gas which can be fairly characterized by the ionization parameter (q). The ionization parameter is given by $q = 10^{\mathrm{A/B}}$, with

$$A = 32.81 - 1.153y^2 + \left[12 + \log(\mathrm{O/H})\right] \times (-3.396 - 0.025y + 0.1444y^2) \tag{B1}$$

and

$$B = 4.603 - 0.3119y - 0.163y^2 + \left[12 + \log(\mathrm{O/H})\right] \times (-0.48 + 0.0271y + 0.02037y^2). \tag{B2}$$

The parameter y is the logarithm of the O_{32} ratio between oxygen lines:

$$y \equiv \log(O_{32}) \equiv \log\left(\frac{I_{[\mathrm{O\,III}]\lambda 4959} + I_{[\mathrm{O\,III}]\lambda 5007}}{I_{[\mathrm{O\,II}]\lambda 3727}} \right), \tag{B3}$$

which is a function of the gas temperature and of its electron density.

The ISM metallicity can be probed with the diagnostic ratio R_{23} given by equation (A3). Using $x \equiv \log \mathrm{R}_{23}$, we have:

$$12 + \log(\mathrm{O/H}) = 9.4 + 4.65x - 3.17x^2 - \log(\mathrm{q}) \times \left(0.272 + 0.547x - 0.513x^2\right) \tag{B4}$$

for $(12 + \log(\mathrm{O/H}) < 8.4)$ and

$$12 + \log(\mathrm{O/H}) = 9.72 - 0.777x - 0.951x^2 - 0.072x^3 - 0.811x^4 - \log(\mathrm{q})$$

Downloaded from https://academic.oup.com/mnras/article-abstract/475/2/1587/4768282 by University of Groningen user on 20 March 2019

$$\times (0.0737 - 0.0713x - 0.141x^2 + 0.0373x^3 - 0.058x^4) \quad \text{(B5)}$$

for $(12 + \log(\mathrm{O/H}) \gtrsim 8.4)$.

An improved estimate of galaxy metallicity can be obtained with a fit from Dopita et al. (2016), given by:

$$12 + \log(\mathrm{O/H}) = 8.77 + \log \frac{I_{[\mathrm{N\,II}]\lambda 6584}}{\mathrm{I}_{[\mathrm{S\,II}]\lambda\lambda 6717.31}} + 0.246 \log \frac{I_{[\mathrm{N\,II}]\lambda 6584}}{I_{\mathrm{H}\,\alpha}}. \quad \text{(B6)}$$

This fit has the advantage of depending only on lines with similar frequencies.

The gas metallicity and the R_{23} ratio can be used to probe the galaxy dust content and, more specifically, the extinction power at the H α frequency. Also, the constraints on the SFRD derived from H α observations are improved by the extra estimate of the strength of the UV field obtained from the ionization parameter and the O_{32} ratio.

Note that the ratio between the H β (468.8 nm) and the O III (500.7 nm) lines, used in the estimation of the R23 ratio, should evolve strongly with redshift. At solar metallicity, the O III line is intrinsically stronger than the H β line. However, like the overall metallicity, the O III line strength relative to the H β line is expected to scale strongly with galaxy mass and to decrease with increasing redshift. Moreover, the amount of doubly ionized oxygen depends on the ionization state of the gas in H II regions. This, in turn, is a function of the density/clumpiness of this gas (Kewley et al. 2013a).

This paper has been typeset from a TEX/LATEX file prepared by the author.

Downloaded from https://academic.oup.com/mnras/article-abstract/475/2/1587/4768282 by University of Groningen user on 20 March 2019